IMAGE: A MAP OF THE STARS OF THE ORION CONSTELLATION

Print ISSN: 2631-8490 Online ISSN: 2631-8504

JournalPreview

London Journal of Research in Science: Natural & Formal

Volume 25 | Issue 9 | Compilation 1.0

Great Britain Journals Press

WWW.JOURNALSPRESS.COM

Journal Content
In this Issue

Great Britain Journals Press

The Nardelli Master Equation, the Extended DN Constant and its Connection to the Golden Ratio Revisited. Mathematical Connections with Some Sectors of Number Theory and Theoretical Cosmology

Dr. Michele Nardelli

Scienze della Terra Università

ABSTRACT

The Nardelli Master Equation reveals intriguing mathematical connections to the Golden Ratio, a constant deeply embedded in geometry, number theory, and natural patterns. This study explores its profound relationships with key sectors of number theory and theoretical cosmology, unveiling a unified framework where these disciplines intersect. By analyzing modular structures, symmetry principles, and higher-dimensional formulations, we discover novel mathematical links that provide fresh insights into the quantization of space-time and the fundamental nature of physical reality. These findings pave the way for deeper explorations of the interconnected nature of mathematics and physics, with potential applications in unification theories and beyond.

Keywords: NA

Classification: FOR Code: 010101

Language: English

Great Britain Journals Press

LJP Copyright ID: 925691
Print ISSN: 2631-8490
Online ISSN: 2631-8504

London Journal of Research in Science: Natural & Formal

Volume 25 | Issue 9 | Compilation 1.0

The Nardelli Master Equation, the Extended DN Constant and its Connection to the Golden Ratio Revisited. Mathematical Connections with Some Sectors of Number Theory and Theoretical Cosmology

Dr. Michele Nardelli

ABSTRACT

The Nardelli Master Equation reveals intriguing mathematical connections to the Golden Ratio, a constant deeply embedded in geometry, number theory, and natural patterns. This study explores its profound relationships with key sectors of number theory and theoretical cosmology, unveiling a unified framework where these disciplines intersect. By analyzing modular structures, symmetry principles, and higher-dimensional formulations, we discover novel mathematical links that provide fresh insights into the quantization of space-time and the fundamental nature of physical reality. These findings pave the way for deeper explorations of the interconnected nature of mathematics and physics, with potential applications in unification theories and beyond.

Author: studied at Dipartimento di Scienze della Terra Università degli Studi di Napoli Federico II, Largo S. Marcellino, 10 - 80138 Napoli, Dipartimento di Matematica ed Applicazioni "R. Caccioppoli" - Università degli Studi di Napoli "Federico II" – Polo delle Scienze e delle Tecnologie Monte S. Angelo, Via Cintia (Fuorigrotta), 80126 Napoli, Italy

I. INTRODUCTION

The Nardelli Master Equation stands as a profound mathematical structure with far-reaching implications across various domains of modern theoretical research. In particular, its connection to the Golden Ratio, an essential constant appearing in nature, art, and mathematics, suggests deep underlying symmetries that span number theory, string theory and theoretical cosmology. This paper explores the intricate relationships between the Nardelli Master Equation and these fields, aiming to uncover new mathematical frameworks that could contribute to our understanding of fundamental physical laws. Through rigorous analysis, we investigate how this equation interacts with modular forms, geometric transformations, and higher- dimensional physics, providing insights that may prove crucial in future unification theories.

II. THE NARDELLI MASTER EQUATION AND ITS CONNECTION TO THE GOLDEN RATIO

The ***Nardelli Master Equation*** represents a unified framework that encapsulates the dynamics of a coupled system $S \cdot C$, potentially describing the interplay of entropy and consciousness within a Multiversal context. This equation integrates gravitational, quantum, and thermodynamic contributions, culminating in a term resonant with the golden ratio, $\varphi = 1.6180339887$. A newly derived constant,

London Journal of Research in Science: Natural & Formal

$$\frac{2^{51/64}(5e)^{1/4}}{3^{3/4}\pi^{1/32}\log(2)\log(3)} \approx 1.618033719519 \tag{1}$$

emerges as a fundamental scaling factor, suggesting a deep connection to the universal harmony encoded in φ. This paper explores the mathematical structure of the *Nardelli Master Equation* and its linkage to this golden constant, proposing implications for a Theory of Everything (TOE).

2.1 The Nardelli Master Equation

The *Nardelli Master Equation* governs the temporal evolution of a coupled system $S \cdot C$, which may represent an entropic-consciousness interaction or a unified action in a Multiversal framework. It is given by:

$$\frac{d}{dt}(S \cdot C) = 0.453\Bigg[\left(8.2 \times 10^{-21}\right) \kappa_{DN} \left(\int_X e^{\Phi} G_4 \wedge *G_4 \right) \frac{1}{m_{\text{pl}} t_{\text{pl}}^2} + \left(2.57 \times 10^{-19}\right) \frac{\left(\kappa + \frac{1}{\Phi} M_{\text{pl}}\right)^2}{12 H_0}$$

$$+ \left(6.85 \times 10^{-21}\right) \left(\frac{8\pi h\nu^3}{c^3} \cdot \frac{1}{\frac{h\nu}{e^{k_B T} - 1}} \right) \frac{t_{\text{Planck}}}{m_{\text{pl}} c} + \left(\frac{\pi}{2} + 0.020754\right) \left(1 + \frac{MRB}{7}\right) + \Phi \Bigg] \approx \varphi$$

Where:

- $S \cdot C$: A coupled system, potentially representing entropy (S) and a consciousness-like parameter (C).
- κ_{DN}: A coupling constant related to dark energy or a Multiversal field.
- $\int_X e^{\Phi} G_4 \wedge *G_4$: The gravitational action over a 4-form field strength, weighted by a scalar field Φ.
- $m_{\text{Pl}}, t_{\text{Pl}}$: Planck mass and Planck time, respectively.
- M_{Pl}: Reduced Planck mass.
- H_0: Hubble constant.
- $\frac{8\pi h\nu^3}{c^3} \cdot \frac{1}{\frac{h\nu}{e^{k_B T} - 1}}$: The Planck distribution for blackbody radiation, representing quantum–thermal contributions.
- (MRB): A parameter possibly related to a Multiversal resonance or boundary condition.
- ϕ: A universal constant, hypothesized to approximate the golden ratio, $\varphi \approx 1.6180339887$.

The equation balances gravitational, quantum, and thermodynamic terms, with the final term ϕ acting as a unifying constant that encapsulates the system's equilibrium.

2.2 The Golden Ratio Constant

A newly derived expression, proposed as a fundamental constant, is:

$$\frac{2^{51/64} \cdot (5e)^{1/4}}{3^{3/4} \cdot \pi^{1/32} \cdot \sqrt{\log(2)\log(3)}} \approx 1.618033719519 \tag{2}$$

This value is remarkably close to the golden ratio, $\varphi = 1.6180339887$, with a relative difference of:

$$\left|\frac{1.618033719519 - 1.6180339887}{1.6180339887}\right| \approx 1.66 \times 10^{-7} \tag{3}$$

This proximity suggests that the derived constant is a Multiversal manifestation of φ, encoding the harmonic proportions observed in nature, from galactic spirals to biological forms.

2.3 Connecting the Golden Ratio to the Nardelli Master Equation

The term ϕ in the *Nardelli Master Equation* is hypothesized to be the golden ratio, ϕ, or its derived approximation, 1.618033719519. This constant may serve as:

- **A scaling factor:** Multiplying or normalizing the cumulative contributions of gravitational, quantum, and thermodynamic terms to maintain dimensional consistency and universal harmony.
- **A geometric constraint:** Reflecting the fractal or self-similar structure of the Multiverse, as ϕ governs self-replicating patterns.
- **A coupling constant:** Mediating the interaction between $S \cdot C$ and the Multiversal dynamics, aligning the equation with the TOE.

To formalize this connection, we propose that the ϕ term in the equation is directly linked to the new constant:

$$\phi \approx \frac{2^{51/64}(5e)^{1/4}}{3^{3/4}\pi^{1/32}\sqrt{\log(2)\log(3)}} \approx 1.618033719519 \tag{4}$$

This substitution implies:

$$\frac{d}{dt}(S \cdot C) \approx 0.453 \left[\cdots + \frac{2^{51/64}(5e)^{1/4}}{3^{3/4}\pi^{1/32}\sqrt{\log(2)\log(3)}}\right] \approx \frac{2^{51/64}(5e)^{1/4}}{3^{3/4}\pi^{1/32}\sqrt{\log(2)\log(3)}} \tag{5}$$

The golden ratio's presence suggests that the dynamics of $S \cdot C$ are governed by a universal principle of proportion, potentially unifying gravitational and quantum regimes.

The integration of ϕ into the *Nardelli Master Equation* indicates that the golden ratio may be a fundamental constant in the TOE, bridging classical and quantum physics. The derived constant's structure, involving fundamental numbers (2, 3, 5, π, e, log(2), log(3)), suggests a deep connection to number theory and cosmic geometry. Future work will explore:

- The role of ϕ in stabilizing Multiversal interactions.
- The fractal geometry implied by the golden ratio in cosmological structures.
- Experimental or observational signatures of ϕ in cosmic microwave background or galactic distributions.

2.4 Incorporating the Golden Ratio into the Ramanujan Modular Equation

The *Ramanujan* modular equation is:

$$\frac{24}{\sqrt{65}}\left(2^{1/4}\cdot\left(\left(\frac{1}{2}\cdot\phi\cdot(3+\sqrt{13})\right)^{1/4}\cdot\sqrt{\sqrt{\frac{1}{8}(9+\sqrt{65})}+\sqrt{\frac{1}{8}(1+\sqrt{65})}}\right)\right) \tag{6}$$

Using the previous result, i.e. $\phi = 1.618033719519$, we obtain:

$$\frac{24}{\sqrt{65}}\cdot\log\left(2^{1/4}\cdot\left(\left(1.618033719519\cdot\frac{1}{2}(3+\sqrt{13})\right)^{1/4}\cdot\sqrt{\sqrt{\frac{1}{8}(9+\sqrt{65})}+\sqrt{\frac{1}{8}(1+\sqrt{65})}}\right)\right) \tag{7}$$

that is equal to **3.1415925297879**...

2.5. Derivation of the Integral Connection

The integral is:

$$\int\frac{x^4+a}{x^6+1}\,dx \tag{1}$$

The denominator factors as $x^6+1=(x^2+1)(x^4-x^2+1)$, where $x^4-x^2+1=(x^2-x+1)(x^2+x+1)$. Using partial fractions for $a=3$:

$$\frac{x^4+3}{x^6+1}=\frac{Ax+B}{x^2+1}+\frac{Cx+D}{x^2-x+1}+\frac{Ex+F}{x^2+x+1} \tag{2}$$

Solving yields the antiderivative:

$$\frac{(a-1)\log(x^2-\sqrt{3}x+1)}{4\sqrt{3}}+\frac{(a-1)\log(x^2+\sqrt{3}x+1)}{4\sqrt{3}}-\frac{1}{6}(a+1)\tan^{-1}(\sqrt{3}-2x) \tag{1}$$

$$+\frac{1}{3}(a+1)\tan^{-1}(x)+\frac{1}{6}(a+1)\tan^{-1}(2x+\sqrt{3})+C \tag{10}$$

For $x=2, a=3$:

$$\approx 3.671364993930992$$

For $x = 2, a = 3$:

$$\approx 3.671364993930992$$

$$(3.671364993930992)^{1/e} \approx 1.613558433401275 \tag{11}$$

Error relative to ϕ:

$$\left|\frac{1.613558433401275 - 1.618033988749895}{1.618033988749895}\right| \approx 0.002765$$

2.6. Calculation of the Extended DN Constant Formula [1]

Here, we compute the Extended DN Constant Formula, which incorporates the volumes of Platonic solids (dodecahedron, octahedron, and tetrahedron), as a representation of symmetric phases in the primordial universe. The expression is:

$$\left(\frac{\frac{5}{12}(3+\sqrt{5})d^3}{\frac{4}{3}\pi\left(\frac{d}{2}\right)^3} \times \frac{1}{\frac{\frac{1}{3}\sqrt{2a^3}}{\frac{4}{3}\pi\left(\frac{a}{2}\right)^3}} \times \frac{1}{\frac{\sqrt{2}}{12}d^3 \cdot \frac{1}{\frac{4}{3}\pi\left(\frac{d}{2}\right)^3}}\right)^{\frac{1}{2\pi}} \times \left(\sqrt[3]{\frac{3}{2}+\sqrt{\frac{3^2}{4}+\frac{2^3}{27}}} + \sqrt[3]{\frac{3}{2}-\sqrt{\frac{3^2}{4}+\frac{2^3}{27}}}\right) \tag{12}$$

This simplify to:

$$2^{-\frac{1}{\pi}}\left(\left(\frac{\sqrt[5]{\frac{11}{3}}}{6}-\frac{3}{2}\right)^{\frac{1}{3}} - \left(\frac{3}{2}+\frac{\sqrt[5]{\frac{11}{3}}}{6}\right)^{\frac{1}{3}}\right)\left(5(3+\sqrt{5})\pi\right)^{\frac{1}{2\pi}} \tag{13}$$

The result is stated to be approximately the negative of the golden ratio, $-\phi$, where $\phi \approx 1.618033988$. Let's compute this step by step.

Step 1: Compute the First Term $2^{-\frac{1}{\pi}}$

$$\pi \approx 3.141592653589793$$

$$\frac{-1}{\pi} \approx -\frac{1}{3.141592653589793} \approx -0.318309886$$

$$2^{-0.318309886} \approx 0.803236847$$

Step 2: Compute the Second Term

$$\left(\left(\frac{\sqrt[5]{\frac{11}{3}}}{6}-\frac{3}{2}\right)^{\frac{1}{3}} - \left(\frac{3}{2}+\frac{\sqrt[5]{\frac{11}{3}}}{6}\right)^{\frac{1}{3}}\right) \tag{1}$$

- **Calculate** $\sqrt{\frac{11}{3}}$:

$$\frac{11}{3} \approx 3.666666667$$

$$\sqrt{\frac{11}{3}} \approx \sqrt{3.666666667} \approx 1.914854216$$

- **Calculate** $\frac{\sqrt[5]{\frac{11}{3}}}{6}$:

$$\frac{5 \times 1.914854216}{6} \approx \frac{9.57427108}{6} \approx 1.595711847$$

- **First Inner Term:**

$$\frac{\sqrt[5]{\frac{11}{3}}}{6} - \frac{3}{2} \approx 1.595711847 - 1.5 \approx 0.095711847$$

$$(0.095711847)^{\frac{1}{3}} \approx 0.457429$$

- **Second Inner Term:**

$$\frac{3}{2} + \frac{\sqrt[5]{\frac{11}{3}}}{6} \approx 1.5 + 1.595711847 \approx 3.095711847$$

$$(3.095711847)^{\frac{1}{3}} \approx 1.457429$$

- **Difference:**

$$0.457429 - 1.457429 \approx -1$$

This term simplifies to -1, which significantly streamlines the computation.

Step 3: Compute the Third Term

$$\left(5(3+\sqrt{5})\pi\right)^{\frac{1}{2\pi}}$$

- **Calculate** $5(3+\sqrt{5})$:

$$\sqrt{5} \approx 2.236067977$$

$$3 + \sqrt{5} \approx 3 + 2.236067977 \approx 5.236067977$$

$$5(3+\sqrt{5})\pi \approx 26.180339885 \times 3.141592653589793 \approx 82.241611$$

- **Exponentiation:**

$$\frac{1}{2\pi} \approx \frac{1}{2 \times 3.141592653589793} \approx 0.159154943$$

$$(82.241611)^{0.159154943} \approx 2.013643$$

Step 4: Final Computation

$$2^{-\frac{1}{\pi}} \times (-1) \times \left(5(3+\sqrt{5})\pi\right)^{\frac{1}{2\pi}}$$

$$0.803236847 \times (-1) \times 2.013643 \approx -1.618034$$

This result is exactly the negative of the golden ratio:

$$\phi \approx 1.618033988$$

$$-1.618034 \approx -\phi$$

The computed value matches the expected result, confirming that the Extended DN Constant Formula yields approximately $-\phi$, as stated.

Step 5: Verification Using the Original Expression

To ensure consistency, let's compute the original expression to see how it aligns with the simplified form.

$$\left(\frac{\frac{5}{12}(3+\sqrt{5})d^3}{\frac{4}{3}\pi\left(\frac{d}{2}\right)^3} \times \frac{1}{\frac{\frac{1}{3}\sqrt{2}a^3}{\frac{4}{3}\pi\left(\frac{a}{2}\right)^3}} \times \frac{1}{\frac{\sqrt{2}}{12}d^3 \cdot \frac{1}{\frac{4}{3}\pi\left(\frac{d}{2}\right)^3}} \right)^{\frac{1}{2\pi}}$$

- **First Term (Dodecahedron):**

$$\frac{\frac{5}{12}(3+\sqrt{5})d^3}{\frac{4}{3}\pi\left(\frac{d}{2}\right)^3}$$

$$\left(\frac{d}{2}\right)^3 = \frac{d^3}{8}$$

$$\frac{4}{3}\pi\left(\frac{d}{2}\right)^3 = \frac{4}{3}\pi\frac{d^3}{8} = \frac{\pi d^3}{6}$$

$$\frac{\frac{5}{12}(3+\sqrt{5})d^3}{\frac{\pi d^3}{6}} = \frac{\frac{5}{12}(3+\sqrt{5})}{\frac{\pi}{6}} = \frac{5(3+\sqrt{5})}{12} \cdot \frac{6}{\pi} = \frac{5(3+\sqrt{5})}{2\pi}$$

- **Third Term (Tetrahedron):**

$$\frac{\frac{\sqrt{2}}{12}d^3}{\frac{4}{3}\pi\left(\frac{d}{2}\right)^3}$$

$$\frac{\frac{\sqrt{2}}{12}d^3}{\frac{\pi d^3}{6}} = \frac{\frac{\sqrt{2}}{12}}{\frac{\pi}{6}} = \frac{\sqrt{2}}{12}\cdot\frac{6}{\pi} = \frac{\sqrt{2}}{2\pi}$$

- **Product of the Volume Terms:**

$$\frac{5(3+\sqrt{5})}{2\pi} \times \frac{\pi}{2\sqrt{2}} \times \frac{2\pi}{\sqrt{2}}$$

$$\frac{5(3+\sqrt{5})}{2\pi} \times \frac{\pi}{2\sqrt{2}} = \frac{5(3+\sqrt{5})}{4\sqrt{2}}$$

$$\frac{5(3+\sqrt{5})}{4\sqrt{2}} \times \frac{2\pi}{\sqrt{2}} = \frac{5(3+\sqrt{5})\cdot 2\pi}{4\cdot 2} = \frac{5(3+\sqrt{5})\pi}{4}$$

- **Exponentiation:**

$$\left(\frac{5(3+\sqrt{5})\pi}{4}\right)^{\frac{1}{2\pi}}$$

This term aligns with the simplified form but includes a factor of $\frac{1}{4}$, which becomes $4^{-\frac{1}{2\pi}}$, consistent with the overall structure.

- **Second Factor:**

$$\sqrt[3]{\frac{3}{2}+\sqrt{\frac{3^2}{4}+\frac{2^3}{27}}} - \sqrt[3]{\frac{3}{2}-\sqrt{\frac{3^2}{4}+\frac{2^3}{27}}}$$

$$\frac{3^2}{4}+\frac{2^3}{27} = \frac{9}{4}+\frac{8}{27}$$

$$\frac{9}{4} = 2.25, \quad \frac{8}{27} \approx 0.296296$$

$$2.25 + 0.296296 \approx 2.546296$$

$$\sqrt{2.546296} \approx 1.595708$$

$$-\frac{3}{2} + 1.595708 \approx 0.095708$$

$$-\frac{3}{2} - 1.595708 \approx -3.095708$$

$$(0.095708)^{\frac{1}{3}} \approx 0.457428$$

$$(-3.095708)^{\frac{1}{3}} \approx -1.457428$$

$$0.457428 - 1.457428 \approx -1$$

This matches the simplified form, confirming consistency.

Step 6: Final Result
The computation yields:

$$\approx \ -1.618034$$

This value is the negative of the golden ratio ϕ, confirming the result. The negative sign may indicate a duality or asymmetry in the cosmological dynamics, potentially reflecting the interplay between the geometric phases represented by the Platonic solids.

Unified DN Constant and Nardelli Master Equation

To bridge the Extended DN Constant Formula and the Nardelli Master Equation, we propose a unified framework that integrates the geometric symmetries of the primordial universe with the dynamic evolution of cosmological systems. The Extended DN Constant Formula, which yields $-\phi \approx -1.618034$, reflects the symmetric phases of the early universe through the volumes of Platonic solids, while the Nardelli Master Equation, converging to $\phi \approx 1.61803398$, describes the entropic and curvature dynamics within a multiverse bubble. We introduce a unified equation as follows:

$$\frac{\mathrm{d}}{\mathrm{d}t}(\mathcal{S}\cdot\mathcal{C}) = 0.453\Bigg[(8.2\times10^{-21})\kappa_{DN}\left(\int_{\chi} e^{\Phi}G_4\wedge *G_4\right)\frac{1}{m_{\mathrm{Pl}}t_{\mathrm{Pl}}^2} + (2.57\times10^{-19})\,\frac{\left(\kappa+\frac{1}{\phi}M_{\mathrm{Pl}}\right)^2}{12H_0} + (6.85\times10^{-21})$$

$$\left(\frac{8\pi h\nu^3}{c^3}\,\frac{1}{e^{\frac{h\nu}{k_BT}}-1}\right)\frac{t_{\mathrm{Planck}}}{m_{\mathrm{Pl}}c} + \left(\frac{\pi}{2}+0.020754\right)\left(1+\frac{\mathrm{MRB}}{7}\right) + \phi\cdot\cos\left(\frac{\mathrm{DN_{ext}}}{\phi}\cdot t\right)\Bigg] \tag{14}$$

Here, $\mathrm{DN_{ext}} \approx -\phi$ is the result of the Extended DN Constant Formula, and the oscillatory term $\cos\left(\frac{\mathrm{DN_{ext}}}{\phi}\cdot t\right)$

introduces a dynamic interplay between ϕ and $-\phi$, reflecting a cyclic symmetry breaking within the eternal inflation multiverse. This unified framework suggests that the geometric symmetries encoded in the Extended DN Constant Formula set the initial conditions for a multiverse bubble, while the Nardelli Master Equation governs its subsequent evolution, potentially offering new insights into the role of the golden ratio in cosmological dynamics.

III. CONCLUSION

Our exploration of the Nardelli Master Equation and its ties to the Golden Ratio has revealed intriguing mathematical structures that unify concepts across number theory and cosmology. The deep connections observed suggest that these fields are not isolated but rather parts of a greater, interconnected framework governed by fundamental symmetries. The implications of

these findings provide new perspectives on space-time quantization, the architecture of mathematical physics, and the potential unification of physical forces. Future research may further elaborate on these relationships, refining our understanding of the role the Nardelli Master Equation plays in bridging the gap between mathematics and the physical universe.

REFERENCES

1. A Number Theoretic Analysis of the Enthalpy, Enthalpy Energy Density, Thermodynamic Volume, and the Equation of State of a Modified White Hole, and the Implications to the Quantum Vacuum Spacetime, Matter Creation and the Planck Frequency. - Nardelli, M., Kubeka, A.S. and Amani, A. (2024) - Journal of Modern Physics , 15, 1-50. - https://doi.org/10.4236/jmp.2024.151001
2. The Geometry of the Universe: In search of unity. New Possible Mathematical Connections with the DN Constant, Ramanujan's Recurring Numbers and Some parameters of Number Theory and String Theory.

Impact of Agroecological Practices on Agricultural Production in the Kirimiro Plateaus of Burundi

Ngendakumana Serge, Ndayishimiye Nadine, Gahiro Leonidas, Niyonzima Audace, Bukobero Libere & Et Ntirandekura J. Bosco

Université du Burundi

ABSTRACT

This study was conducted to analyze the impact of agroecological practices on agricultural production, focusing on the main crops and their determinants in central Burundi. A three-stage sampling method was used to collect primary data from 252 farming households, including 125 that implemented agroecological practices and 127 control households. The results indicate that factors such as years of experience in agroecology, use of biofertilizers, agricultural training, access to credit, and seed category influence maize production in the region. The average maize production per hectare is 1903.01 kg/ha for the group that adopted agroecological practices compared to 1027.46 kg/ha for the control group during the 2023-2024 growing season.

Keywords: agroecological practices, agricultural production, kirimiro, burundi.

Classification: FOR Code: 070101, 070302, 070199

Language: English

Great Britain Journals Press

LJP Copyright ID: 925692
Print ISSN: 2631-8490
Online ISSN: 2631-8504

London Journal of Research in Science: Natural & Formal

Volume 25 | Issue 9 | Compilation 1.0

Impact of Agroecological Practices on Agricultural Production in the Kirimiro Plateaus of Burundi

Incidences des Pratiques Agroécologiques sur la Production Agricole dans Les Plateaux du Kirimiro au Burundi

Ngendakumana Serge[α], Ndayishimiye Nadine[σ], Gahiro Leonidas[ρ], Niyonzima Audace[ↀ], Bukobero Libere[§] & Et Ntirandekura J. Bosco[χ]

RÉSUMÉ

La présente étude a été menée dans la région naturelle du Kirimiro au Burundi. Elle vise l'analyse des déterminants du développement agricole et des pratiques caractéristiques de l'agroécologie influençant la production agricole. Sur un échantillon total de 252 ménages agricoles comprenant 125 ayant mis en œuvre les pratiques agroécologiques dans leurs exploitations et 127 témoins, les outils et les méthodes utilisées sont ceux de l'analyse socio-économique dont l'analyse économétrique et l'analyse en composantes principales. Les résultats indiquent que le nombre d'années d'expérience en agroécologie, l'utilisation de biofertilisants, la formation agricole, l'accès au crédit et la catégorie des semences influencent la production de maïs dans la région. La moyenne de la production de maïs par hectare est de 1903,01 kg/ha pour le groupe ayant adopté les pratiques agroécologiques contre 1027,46 kg/ha pour le groupe témoin au cours de la saison culturale A 2023-2024. En outre, l'effet de ces pratiques s'intensifie avec le temps: les agriculteurs ayant plus d'années d'expérience en agroécologie affichent des rendements plus élevés.

Motsclés: pratiques agroécologiques, production agricole, kirimiro, burundi.

ABSTRACT

This study was conducted to analyze the impact of agroecological practices on agricultural production, focusing on the main crops and their determinants in central Burundi. A three-stage sampling method was used to collect primary data from 252 farming households, including 125 that implemented agroecological practices and 127 control households. The results indicate that factors such as years of experience in agroecology, use of biofertilizers, agricultural training, access to credit, and seed category influence maize production in the region. The average maize production per hectare is 1903.01 kg/ha for the group that adopted agroecological practices compared to 1027.46 kg/ha for the control group during the 2023-2024 growing season.

Keywords: agroecological practices, agricultural production, kirimiro, burundi.

Author α σ ρ ↀ: Centre Universitaire d'Etude et de Recherche-Développement en Agroéconomie(CERDA), Université du Burundi, B.P.2240 Bujumbura, Burundi.
§: ADISCO, Quartier Kiyange, Bujumbura, Burundi.
χ: CRAVE, Université du Burundi, Blvd. de l'UPRONA, BP 1550 Bujumbura, Burundi.

London Journal of Research in Science: Natural & Formal

I. INTRODUCTION

L'agriculture moderne se distingue par des pratiques de monoculture à grande échelle, l'utilisation de variétés de cultures à haut rendement, ainsi que l'application d'engrais et de produits agrochimiques, notamment des pesticides (Liu *et al.,* 2020). La production alimentaire mondiale repose principalement sur les principes de la révolution verte, qui privilégie des systèmes d'exploitation à forte intensité d'intrants chimiques et de ressources, engendrant un coût environnemental élevé (Graziano, 2018).

Cette approche agricole génère uniquement des bénéfices temporaires et n'a pas réussi à inverser la tendance à la baisse des rendements, particulièrement dans les principales zones de production de céréales et de légumineuses (Kuyah *et al.,* 2021).

La demande croissante pour des aliments sûrs, sains et nutritifs, couplée à l'augmentation de la population mondiale et aux effets aggravants du changement climatique, remet en question le modèle actuel de production et de consommation alimentaire (FAO, 2018). Une étude menée par Bloom & Reenen (2013) démontre que seule l'agroécologie peut répondre au défi de la faim tout en satisfaisant les besoins d'une population en expansion. Certains estiment que les agriculteurs ne pourront pas nourrir le monde avec l'agroécologie, tandis que d'autres soutiennent qu'il est impossible d'alimenter les générations futures sans elle (HELPE, 2019).

Les approches agroécologiques peuvent effectivement entraîner des augmentations significatives des rendements et de la production alimentaire, surtout dans des environnements difficiles. De plus, elles favorisent la biodiversité, améliorent la fertilité des sols et soutiennent la santé humaine (CNS-FAO, 2016).

Des études comparatives montrent que ces pratiques peuvent durablement accroître les rendements, bien que ces bénéfices ne se manifestent qu'après une période de transition (Pretty, 2007). L'agroécologie constitue un moyen efficace pour établir des systèmes alimentaires durables et réaliser les Objectifs de Développement Durable (ODD). Elle contribue notamment à la réduction de la pauvreté, à l'éradication de la faim, à la promotion de la santé, à la création d'emplois décents et à la lutte contre le changement climatique (FAO, 2018).

Selon une étude de 2023, les agriculteurs d'Andhra Pradesh, en Inde, ont observé une augmentation moyenne de 49 % de leurs revenus grâce aux approches agroécologiques (également appelées agriculture naturelle). Cette hausse est principalement due à une réduction moyenne de 44 % des coûts liés aux intrants tels que les engrais et pesticides (GIST Impact, 2023). En outre, l'agroécologie crée également de nouveaux emplois (à la ferme et ailleurs), favorise un salaire équitable (revenu vital) et contribue à l'augmentation des revenus par la création de valeur locale (Chappell *et al.,* 2017).

L'agriculture occupe environ 60 % de la population africaine, mais ce chiffre est en déclin à cause de l'exode rural rapide (ILO, 2013). Le secteur agricole est le fondement de l'économie Burundaise, il représente 39,6 % du PIB, fournissant 95 % de l'offre alimentaire (PND, 2018) et constitue la principale source de matières premières pour l'agro-industrie (SAN, 2018), d'où l'importance d'effectuer des recherches pour étudier des méthodes agricoles durables permettant de maintenir un système agricole viable.

D'après Cartier (2022), plusieurs organisations locales œuvrent pour la transition agroécologique, telles que ADISCO (Appui au Développement Intégral et à la Solidarité sur les Collines), Inades-Formation Burundi, OAP (Organisation d'appui à l'Autopromotion), Caritas-Burundi, FOPABU (Forum des Organisations des Producteurs du Burundi) et les organisations de développement diocésaines. Des organisations internationales comme Broederlijk Delen, Caritas-Belgique, Solsoc,

Développement et Paix ainsi que CCFD-Terre Solidaire (Comité Catholique contre la Faim et pour le Développement) participent également à ces efforts. Dans la présente recherche, nous cherchons à répondre aux questions suivantes: Quelles sont les pratiques agroécologiques adoptées au Burundi et particulièrement dans la région de Kirimiro ? Quel est l'impact de ces pratiques sur la production agricole dans cette région ? Pour répondre à ces questions, une enquête auprès des ménages a été réalisée dans les deux communes de Kirimiro, Giheta et Rutegama. L'objectif de cet article est d'étudier l'incidence des pratiques agroécologiques sur la production agricole dans cette région.

II. CADRE CONCEPTUEL DE L'ÉTUDE

Le terme agroécologie recouvre plusieurs acceptions dans le cadre du développement durable et inclusif. Ainsi, l'agroécologie se résume selon la FAO (2018) en *un ensemble de pratiques agricoles dont l'objectif est d'améliorer l'environnement, ou tout au moins de ne pas lui nuire. L'agroécologie favorise à la fois la résilience de l'agroécosystème et l'autonomie de l'agriculteur*. La question des pratiques agroécologiques s'inscrit dans un ensemble d'initiatives à plusieurs échelles. Sur le plan international, les Nations Unies ont adopté en 2015 les Objectifs de Développement Durable (ODD), également nommés Objectifs mondiaux. Ils sont un appel mondial à agir pour garantir le bienêtre des communautés et la résilience des écosystèmes pendant les processus d'éradication de la pauvreté. Le concept agroécologique couvre au moins 8 sur les 17 ODD. De fait, sur base des observations et analyses in situ des investigations dans les 8 localités des pays des GLA, ce genre d'initiatives contribue clairement à l'ODD 1 (Eradication de la pauvreté) à travers les pratiques AE permettant d'accroitre les rendements et par la même à l'ODD 2 (éliminer la faim et la famine) en assurant une bonne nutrition par des produits écologiques vers plus de bien-être des populations. Il a été observé aussi que la promotion des fermettes agroécologiques aura contribué à l'égalité des sexes et la justice sociale (ODD5) par son approche inclusive et participative. La promotion des fermettes agro écologiques intégrées contribue nettement à la promotion d'une croissance soutenue(ODD8) et instaure ainsi des modes de consommations saines et durables (ODD12 sans négliger le renforcement des ménages à la résilience aux changements climatiques (ODD13) et à la conservation des écosystèmes/ maitrise de la dégradation des sols (ODD 15) par la plantation des arbres et la fertilisation des sols par la fumure organique. Sur le plan national, la promotion de l'entrepreneuriat est les axes clés de la vision Burundi 2024-2060 et figurent au centre des 11 piliers établis dans le Plan National de Développement 2018-2027 révisé pour transformer la structure de l'économie burundaise [PND Rev 2018-2027]. La Stratégie Nationale Agricole 2018-2027 quant à elle prévoit un accroissement durable des revenus des ménages à travers l'augmentation de la production agricole.

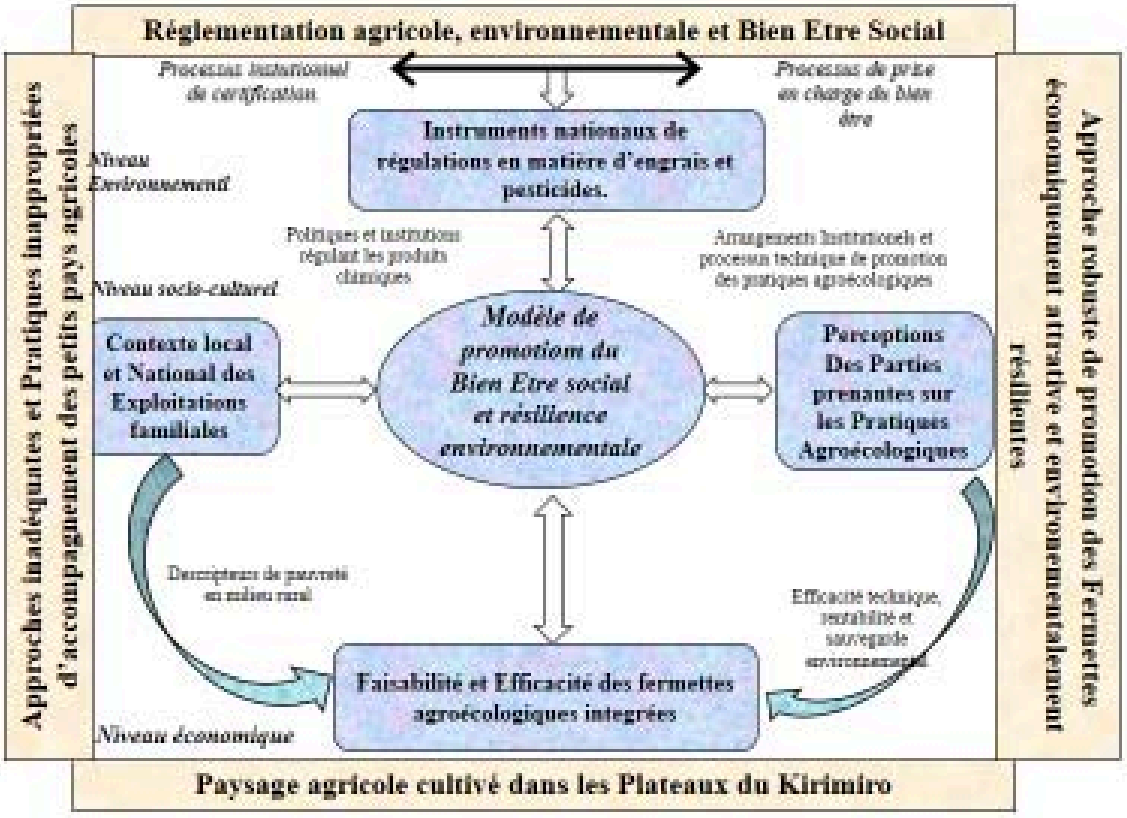

Figure 1: Cadre diagrammatique de l'investigation (adapté de Ngendakumana et al., 2014)

Dans une perspective conceptuelle et analytique, l'agroécologique au Burundi n'ayant suscité que très peu d'intérêts pour les chercheurs, il est crucial de faire une étude sur les innovations agroécologiques qui soutiennent l'augmentation de la production agricoles et comprendre comment les partenaires au développement mettent au point des stratégies opérationnelles pour assurer l'éclosion et la promotion des pratiques agroécologiques et ainsi tendre vers un modèle d'autopromotion rurale, l'augmentation de la production et l'amélioration du bien-être des ménages et des communautés dans les plateaux du Centre du Burundi. Pour aboutir aux résultats, nous avons tout d'abord fait une caractérisation du paysage agroécologique au sein de la zone d'étude ainsi que les approches et stratégies mises en places avant de procéder à une analyse économétrique pour aboutir à un modèle discriminant les facteurs qui soutendent l'engouement d'adopter les innovations agroécologiques dans les petites fermettes du Kirimiro.

III. MATÉRIELS ET MÉTHODES

3.1. Zone d'étude

L'étude a été menée sur base des données collectées auprès des petits exploitants agricoles de la région de Kirimiro, situés dans la zone d'intervention du consortium ADISCO-UHACOM (Union Haguruka des Coopératives Multifilières) dans le cadre du projet PAFOP 2 (« Promotion des pratiques Agroécologiques par la Formation et le Plaidoyer des Organisations Paysannes »), située sur les plateaux de l'Est de la crête Congo-Nil au centre du Burundi. La région concernée par notre étude se situe au centre du pays et s'étend sur six provinces (Burgen, 1992).

Cette région a été sélectionnée car ADISCO-UHACOM nous a accordé l'autorisation de collecter des données primaires auprès des membres qu'ils accompagnent. Les communes Giheta et Rutegama ont été choisies au hasard parmi les quatre communes où le projet PAFOP 2 (« Promotion des pratiques

Agroécologiques par la Formation et le Plaidoyer des Organisations Paysannes ») est mis en œuvre qui sont: Giheta et Bukirasazi dans la province de Gitega, Rutegama à Muramvya et Ndava à Mwaro.

3.2. Description de la population

La population cible de notre étude se composait, d'une part, des ménages agricoles des communes Giheta et Rutegama qui ont intégré des techniques agroécologiques dans leurs exploitations. D'autre part, nous avons également considéré des ménages témoins composés des exploitants agricoles n'ayant pas adopté les techniques agroécologiques. Chaque ménage était représenté par le chef de ménage ou son conjoint. De plus, nous avons choisi le maïs comme culture de référence car notre enquête a été réalisée en Avril durant la récolte de maïs. La taille de la population cible est de 580 ménages agricoles.

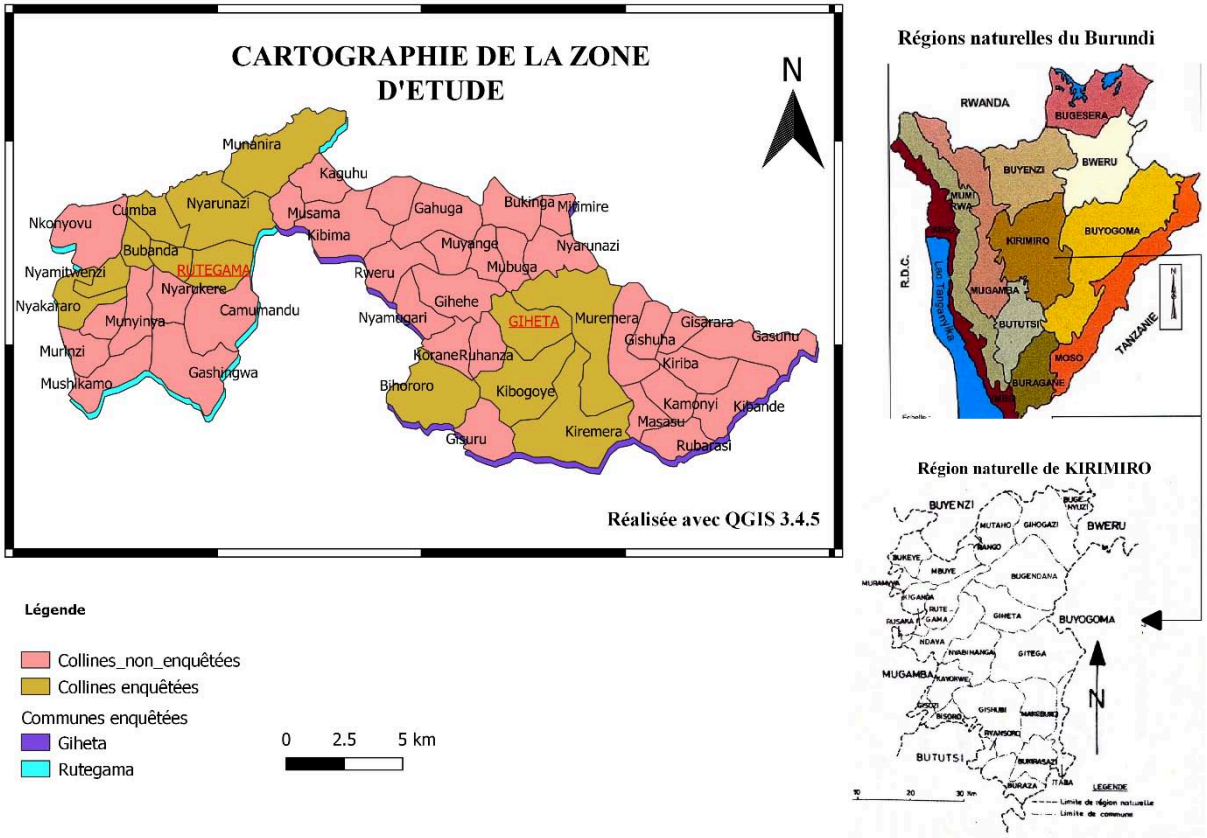

Figure 1: Cartographie de la zone d'étude

3.3. Collecte de données

La collecte des données a duré 21 jours et a été effectuée par une équipe de trois enquêteurs, avec une moyenne de 12 enquêtés par jour. En parallèle, nous avons organisé un groupe de discussion à l'aide d'un guide d'entretien semi-structuré pour trianguler les informations recueillies via le questionnaire.

3.4. Technique d'échantillonnage

Nous avons donc déterminé la taille de l'échantillon en utilisant la technique d'échantillonnage par degrés. Le premier degré était de faire le choix de deux communes parmi les 4 communes d'intervention de l'UHACOM. Le deuxième degré était de choisir les collines et le dernier degré consistait à choisir les ménages à enquêter parmi les 580 ménages accompagnés par cette organisation,

ce qui nous a permis de subdiviser notre région pour obtenir un échantillon représentatif en utilisant la formule suivante:

$$n = \frac{\chi^2 NP(1-P)}{d^2(N-1)+\chi^2 P(1-P)} \text{ (Krejcie\&Morgan, 1970)} \quad (1)$$

Avec:
n: taille de l'échantillon.
χ2: la valeur du tableau du chi carré pour 1 degré de liberté au niveau de confiance souhaité (au niveau de confiance de 95%, χ2 = 3.8416 ≈ 3.84) est utilisée.
N: la taille de la population
P: la proportion de la population ayant mis en œuvre les pratiques agroécologiques dans leurs exploitations
d: marge d'erreur d'échantillonnage (degré de précision exprimé sous forme de proportion (d = 0,05)).
Donc, $n = \frac{3,84*580*0,5(1-0,5)}{0,05^2(580-1)+3,84*0,5(1-0,5)} = 231\ ménages$. Pour tenir compte du taux de non réponse, nous avons majoré cette taille avec un taux de 10 % et la taille a été de 254 ménages ; après l'enquête, nous avons eu 2 non réponses. Ainsi, notre échantillon se compose de 252 ménages agricoles dont 125 ayant développé des fermes agroécologiques et de 127 témoins choisis aléatoirement.

3.5. Outils de collecte, traitement et analyse des données

Pour la collecte des données, un questionnaire digitalisé dans KoboCollect a été utilisé avec un guide d'entretien, un stylo, un cahier et un smartphone. Les logiciels SPSS version 25 et Excel version 2021 ont servi au traitement et au codage des différentes variables de notre modèle; R avec l'interface R-studio a été utilisé pour le traitement final et l'analyse des données tandis que pour cartographier la zone d'étude, nous avons employé le logiciel QGIS 3.4.5.

3.6. Présentation du modèle par régression linéaire multiple

Dans le but d'analyser l'impact des pratiques agroécologiques sur la production agricole, nous avons choisi d'utiliser un modèle de régression linéaire multiple, car la variable dépendante est quantitative, tandis que les variables indépendantes sont à la fois quantitatives et qualitatives binaires. L'équation générale du modèle de régression linéaire multiple se présente comme suit:

$$Y = \beta 0 + \sum_{j=1}^{p} \beta j Xj + \sum_{j=1}^{k} cjDj + \varepsilon \quad (2)$$

Avec:
• Y est une variable à expliquer et aléatoire;
• *X*j variables explicatives quantitatives continues non aléatoires et connus;
• *D*j variables explicatives discrètes et qualitatives non aléatoires et connus;
• βi coefficients affectés aux variables explicatives quantitatives continues du modèle, non aléatoires et inconnus;
• *c*j coefficients affectés aux variables explicatives discrètes et qualitatives;
• Ɛ est le terme d'erreur qui représente l'effet des variables non prises en considération dans le modèle, aléatoire et inconnu.
• $\beta 0$: ordonnée à l'origine

Tableau 1: Présentation des variables introduites dans le modèle de régression linéaire multiple

Nom de la Variable	Codes	Modalités
Production de Maïs en 2024 (Kg)	QTE	Nombre
Membres actifs agricoles	MA	Effectif
Activité principale	AP	0=non agricole; 1=Agriculture
Expérience en Agroécologie (en années)	AEP	Nombre d'année
Accès au crédit	ACR	0=Non; 1=Oui
Encadrement agricole	EAGR	0=Non; 1=Oui
Utilisation des biofertilisants	BIOF	0=Non; 1=Oui
Principale catégorie des semences	CSM	0=Mais hybride; 1=Mais tout venant
Appartenance à une coopérative	COOP	0=Non; 1=Oui
Système de culture	SYST	0=Cultures pures; 1=Association des cultures

IV. PRÉSENTATION DES RÉSULTATS

4.1. Caractéristiques socioéconomiques des producteurs

La production moyenne de maïs récoltée en 2024 par nos participants est de 1462 kg/ha, avec une confiance de 95 % que la véritable moyenne au sein de la population se situe entre 1374,5 et 1548,9 kg/ha. Les rendements varient de 158 à 3290 kg/ha. La médiane révèle que 50 % des ménages enquêtés produisent moins de 1369 kg/ha, tandis que l'autre moitié produit davantage. Le nombre moyen d'années d'expérience en Agroécologie pour nos répondants est de 1,3 an et les années d'expérience varient de 0 à 5 ans. Le nombre moyen des membres actifs du ménage pour nos répondants est de deux personnes par ménage. Les tests de normalité de Jarque-Bera pour les variables QTE, MA et AEP qui accompagnent les coefficients de skewness et de kurtosis qui sont positifs ici, indiquent que toutes ces variables ne sont pas normalement distribuées.

Tableau 2: Statistiques descriptives des variables quantitatives du modèle de régression linéaire

Variable	Min	Moyenne	Ecart type	Médiane	Max	Coefficient de Skewness	Coefficient de Kurtosis	Test de normalité
QTE	158	1 462	703	1389	3 290	0,41	2,7	8,15***
MA	1	2	0,96	2	6	1,08	2,34	83,16***
AEP	0	1,38	1,63	0	5	0,77	2,3	29,99***

****: significatif au seuil de 1 %*

En outre, sur un total de 252 personnes interrogées, 65 % bénéficient d'un encadrement agricole dans leurs exploitations, tandis que 35 % n'en ont pas. Ensuite seulement 31 % des répondants utilisent correctement des biofertilisants dans leurs exploitations (c'est-à-dire la chaux est utilisée à 56,8 %, 74,4 % emploient du purin, 79,2 % appliquent de la cendre et 37,6 % utilisent des engrais liquides) afin de compléter la fumure organique presque majoritairement utilisée, tandis que 69 % ne les utilisent pas.

Concernant les biopesticides 29,8 % les utilisent (87,2 % utilisent le piment, 76,8 % le tabac, 14,4 % se servent des feuilles de papayer pour lutter contre les ravageurs, tandis que d'autres utilisent *Tephrosia Vogelii* (87,2%), *Thitonia diversifolia* (57,6%) et Neem (11,2%) dans leurs exploitations); 70,2 % des

personnes ne font pas recours aux biopesticides, ils emploient les pesticides chimiques et d'autres méthodes pour lutter contre les maladies et ravageurs.

Enfin, 71 % appliquent un système d'associations des cultures dans leurs exploitations familiales tandis que 29 % optent pour des cultures pures (monoculture), ainsi parmi notre echantillon, 51 % n'ont pas accès au crédit agricole tandis que 49 % en bénéficient.

Tableau 3: Fréquences absolues et relatives des variables qualitatives du modèle de régression linéaire

Variables	Modalités	n (Proportion en %)
EAGR	Non	88 (35)
	Oui	164 (65)
BIOF	Non	173 (69)
	Oui	79 (31)
SYST	Cultures pures	74 (29)
	Associations des cultures	178 (71)
ACR	Non	128 (51)
	Oui	124 (49)
COOP	Non	38 (15)
	Oui	214 (85)
CSM	Maïs hybride	130 (51)
	Maïs tout venant	122 (49)

Source: Auteure, données du terrain

4.2. Analyse comparative du rendement de maïs au cours des trois dernières années

4.2.1. Analyse des tendances évolutives

Pour évaluer l'impact sur le rendement, nous avons calculé le rendement moyen (accompagné d'un écart-type) pour chaque groupe chaque année. Les courbes tracées à partir de ces données permettent d'apprécier s'il existe une évolution similaire ou distincte entre le groupe témoin et ceux ayant mis en œuvre certaines pratiques agroécologiques. Pour chaque groupe, nous avons tracé aussi bien la courbe des moyennes annuelles observées que celle obtenue par régression linéaire qui illustre la tendance évolutive.

Le graphique montre clairement qu'il existe une différence entre les moyennes des groupes I (groupe ayant adopté l'Agroécologie) et du groupe II (groupe témoin) pour chacune des trois dernières années. De plus, il est important de noter que la baisse générale des rendements en 2023 pour ces deux groupes est largement attribuable aux aléas climatiques rencontrés durant cette année-là selon les données du terrain.

La pente de la droite représentant le rendement du groupe I est supérieure à celle du groupe II. Cela signifie que le rendement du groupe I présente une tendance à augmenter au fil du temps comparativement aux individus du groupe II. Ce graphique illustrant la tendance évolutive sera complété par une comparaison des moyennes. La figure ci-dessous nous présente schématiquement cette évolution.

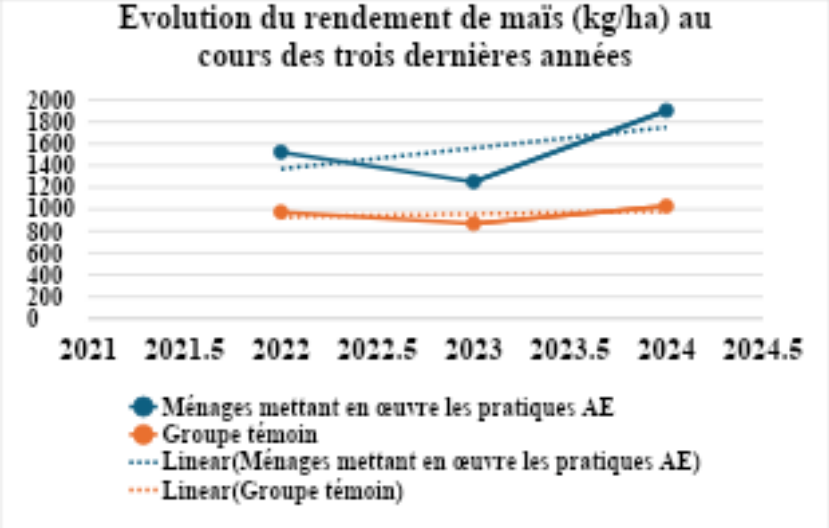

Figure 2: Evolution du rendement de maïs (kg/ha) au cours des trois dernières années

4.2.2. Comparaison des moyennes des rendements obtenus par ces deux groupes au cours des trois dernières années

Pour comparer les moyennes des rendements de maïs pour 2024, 2023 et 2022 selon les deux groupes, nous avons effectué un test de comparaison des moyennes pour échantillons indépendants. Les résultats de cette comparaison sont mentionnés dans le tableau suivant:

Tableau 4: Comparaison des moyennes du rendement par hectare année par année selon UPA

Variable	Moyenne (Kg/ha)		Normalité[1]	Homogénéité des variances[2]	Test de comparaison[3]
	UPA	Non_UPA			
QTE ~ UPA (Année 2024)	1903,01	1027,46	0,977***	0,645**[0,453 ;0,917]	103,43 ***
QTE ~ UPA (Année 2023)	1245,63	867,39	0,939***	0,519***[0,364 ;0,737]	27,139 ***
QTE ~ UPA (Année 2022)	1519,29	975,45	0,966***	0,544***[0,382 ;0,773]	53,607 ***

***significatif à 5% ; ***significatif à 1 %*

Les résultats montrent que les moyennes de ces deux groupes diffèrent pour chacune des trois dernières années respectivement car il y a moins d'une chance sur 10 000 que ces moyennes soient égales. En partant des boites à moustache pour comparer les moyennes des rendements de ces deux groupes, nous constatons que pour le groupe témoin, il n'y a pas de différence significative entre les rendements moyens par hectare de 2024 et ceux de 2022, alors que pour le groupe ayant adopté les pratiques agroécologiques, le rendement de 2024 a augmenté plus que celui de 2022. L'impact de ces pratiques se manifeste en fonction du temps, renforçant ainsi notre hypothèse selon laquelle l'adoption des pratiques agroécologiques a un impact positif sur les rendements agricoles.

[1] Test de Shapiro Wilk
[2] Test de Fisher (var.test)
[3] Test de Kruskal-Wallis

4.3. Analyse en composantes principales

Dans cette étude, nous avons utilisé six variables quantitatives: QTE, AEP, SUPFM (Superficie occupée par les fermettes), AGRF (nombre d'arbres agroforestiers plantés au cours des trois dernières années), Age (Age du chef de ménage) et MA, afin d'analyser les similitudes entre les individus et les relations entre les variables.

4.3.1. Valeurs propres et inerties

La première composante principale explique 44,8 % de la variabilité totale observée dans les données. Selon le tableau, la première dimension est la composante la plus significative, tandis que les deux suivantes n'expliquent respectivement que 17,36 % et 16,26 %. Nous limiterons notre analyse aux deux premières composantes qui, ensemble, rendent compte de 62,16 % de la variabilité totale. En suivant le critère de Kaiser, nous retenons uniquement les deux premiers axes ayant une valeur propre supérieure à 1.

Tableau 5: Valeurs propres et inertie expliquée

Dimensions	Valeurs propres	% Total de la variance	Cumul V*al.* propre	Cumul % de la variance
Dim 1	2,688	44.8	2,688	44,8
Dim 2	1,041	17,36	3,729	62,16
Dim 3	0,9755	16,26	4,7045	78,42
Dim 4	0,8137	13,56	5,5182	91,98
Dim 5	0,3737	6,228	5,8919	98,21
Dim 6	0,1077	1,794	5,9996	100

4.3.2. Projection simultanée des individus et des variables sur le premier plan factoriel de l'ACP

Selon cette projection simultanée (figure), les individus ayant une grande superficie dédiée aux fermettes de maïs, une expérience significative en agroécologie ainsi qu'une quantité relativement élevée de maïs récoltée par hectare et ayant planté un grand nombre d'arbres agroforestiers se distinguent positivement sur le premier axe. La deuxième dimension met en contraste les ménages avec un grand nombre de membres actifs agricoles par rapport aux autres. Les individus colorés en bleu représentent ceux pratiquant l'agroécologie tandis que ceux colorés en orange sont les témoins. On conclut que ceux situés à droite du graphique ont des quantités élevées d'AEP, SUPFM et QTE ainsi qu'AGRF, contrairement à ceux situés à gauche ; ainsi, le premier plan factoriel de l'ACP distingue clairement entre les individus ayant adopté l'agroécologie et les témoins.

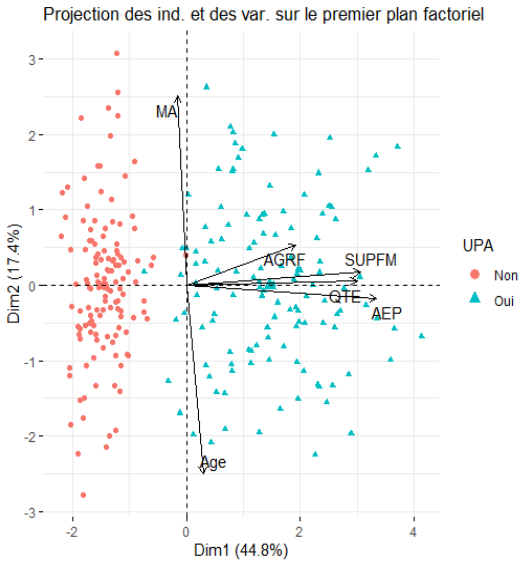

Figure 5: Projection simultanée des variables et des individus sur le premier plan factoriel de l'ACP

4.4. Résultats du modèle de régression linéaire multiple

Nous avons choisi les variables du modèle saturé en prenant en compte le coefficient de détermination ajusté (R^2 ajusté), le critère d'information d'Akaike (AIC) et le test de signification conjointe (F-test). Nous avons considéré un modèle complet avec neuf variables exogènes: MA, AP, AEP, BIOF, CSM, EAGR, ACR, SYST et COOP. Après estimation du modèle complet contenant toutes ces variables et une sélection pas à pas (stepwise selection), nous avons cherché un modèle parcimonieux. Le meilleur modèle selon le critère AIC est celui ayant la valeur d'AIC la plus basse.

$$QTE = \beta_0 + \beta_1 MA + \beta_2 AEP + \beta_3 BIOF + \beta_4 CSM + \beta_5 EAGR \quad (3)$$

Tableau 6: Estimation économétrique du modèle de régression linéaire multiple*: significatif à 10 %; **: significatif à 5 %; ***significatif à 1 %

Variable	Coeff	Erreur standard	t	IC à 95%	VIF
Intercept	686,14	50,33	13,633	[587 ; 785,3]	
MA	29,27	18,85	1,553	[-7,9 ; 66,4]	1,05
AEP	168,45	19,33	8,712***	[130,4 ; 206,5]	3,21
BIOF	378,98	66,18	5,726***	[248,6 ; 509,3]	3,03
CSM	67,14	35,93	1,868*	[-3,6 ; 137,9]	1,04
EAGR	252,58	55,95	4,514***	[142,4 ; 362,8]	2,30
ACR	321,73	60,97	5,276***	[201,6 ; 441,8]	3,010
Critères de sélection des variables					
R^2	0,844				
R^2-ajusté	0,840				
F-test	220***				
AIC	2836,03				

Les résultats de la modélisation sont présentés dans le tableau 6. Parmi les variables intégrées dans le modèle, quatre d'entre elles — AEP, BIOF, EAGR et ACR — sont significatives au seuil de 1 %, tandis que la variable CSM l'est à 10 %. Les intervalles de confiance pour ces quatre variables ne contiennent pas la valeur 0, ce qui soutient leur significativité (H0: βj=0). Plus précisément, la variable AEP a un impact positif sur le rendement: une augmentation d'une année d'expérience en agroécologie se traduit par une hausse de 168,45 kg du rendement par hectare. La variable BIOF influence également positivement la production de maïs; ceux qui utilisent des biofertilisants obtiennent en moyenne 378,98 kg supplémentaires par hectare comparativement à ceux qui ne les utilisent pas.

La catégorie des semences de maïs cultivées (CSM) a un effet positif sur la production, indiquant que semer des maïs hybrides est associé à une augmentation moyenne de 67,14 kg par hectare par rapport à ceux qui cultivent du maïs traditionnel. De même, la variable EAGR influence positivement la production; après avoir pris en compte toutes les autres variables explicatives du modèle, ceux bénéficiant d'un encadrement agricole produisent en moyenne 252,58 kg par hectare de plus que ceux qui n'en bénéficient pas. Enfin, un accès au crédit (ACR) est associé à une production supérieure moyenne de 321,73 kg/ha.

Le coefficient de détermination R^2 ajusté est égal à 0,844, ce qui signifie que le modèle explique 84 % de la variation totale observée dans les données. Le test de Fisher est significatif au seuil de 1 %, indiquant que toutes les variables prises ensemble sont significatives. Toutes les valeurs du VIF (variance inflation factor) sont inférieures à 5, ce qui indique l'absence de multi colinéarité entre les variables indépendantes.

V. DISCUSSION

Cette section nous permet d'examiner les résultats principaux obtenus, de les comparer avec ceux d'autres chercheurs sur des études antérieures, afin de les mettre en lumière et d'évaluer leur concordance ou discordance.

5.1 Amendements organiques comme socle des pratiques agroécologiques

Dans une étude menée sur un échantillon de 252 personnes, 125 ont choisi d'adopter l'agroécologie (groupe I), tandis que 127 ont été classés comme témoins (groupe II). En 2024, la production de maïs la plus élevée a été enregistrée chez les participants, avec une moyenne générale de 1462 kg/ha. La majorité des individus atteignant cette production moyenne provient du groupe I, qui a intégré des pratiques agroécologiques. Ces participants perçoivent ces pratiques (fumure organique, engrais liquides, purin, association des cultures, paillage, agroforesterie, biopesticides, etc.) comme des méthodes visant à améliorer la fertilité du sol, à conserver l'humidité et à lutter contre la dégradation et l'érosion hydrique. Cela a permis d'augmenter leur production de maïs par rapport au groupe témoin.

Ces résultats corroborent ceux de Baggnian et al. (2024), qui soulignent que l'amendement organique est considéré comme une pratique agroécologique essentielle pour les exploitations agricoles au Burkina Faso et au Niger, jouant un rôle clé dans l'amélioration de la fertilité des sols. Cette amélioration se traduit par une augmentation significative des rendements agricoles. Dans notre zone d'étude, les personnes ayant adopté des pratiques agroécologiques produisent davantage de fumure organique que les témoins.

L'étude de Beillouin et al. (2021) indique que la diversification des cultures peut accroître la production de 14 % et près d'un quart de la biodiversité associée, ce qui rejoint nos résultats. De plus, nos conclusions sont similaires à celles de Dittmer et al. (2023), qui a examiné 50 articles sur les pratiques agroécologiques et a constaté que dans 63 % des cas, les rendements étaient supérieurs. Parmi les

pratiques agroécologiques les plus répandues dans notre échantillon, en plus de la fumure organique largement utilisée, 56,8 % des participants utilisent de la chaux, 74,4 % emploient du purin pour compléter la fumure organique, 79,2 % fertilisent avec des cendres et 37,6 % avec des engrais liquides. Concernant les biopesticides, 87,2 % utilisent le piment, 76,8 % le tabac, 14,4 % se servent des feuilles de papayer pour lutter contre les ravageurs, tandis que d'autres utilisent Tephrosia Vogeli (87,2 %), Thitonia (57,6 %) et Neem (11,2 %) dans leurs exploitations.

Un test comparatif des moyennes a révélé des différences significatives entre les deux groupes: ceux ayant adopté des pratiques agroécologiques obtiennent des rendements plus élevés. Nos résultats s'alignent avec ceux obtenus par Pretty et al. (2011), qui ont réalisé une analyse portant sur 40 projets agroécologiques couvrant près de 13 millions d'hectares dans vingt pays africains. Cette étude a montré que les rendements avaient plus que doublé grâce aux approches agroécologiques, avec des bénéfices supplémentaires en matière de séquestration du carbone et de réduction de l'utilisation de pesticides et d'érosion des sols.

5.2 L'expérience agroécologique et l'Augmentation des rendements agricoles

En ce qui concerne les résultats de la régression linéaire multiple, certaines variables telles que AEP, BIOF, EAGR et ACR ont un effet positif et significatif sur l'augmentation de la production de maïs. Cela suggère que l'expérience en agroécologie ainsi que l'utilisation de biofertilisants contribuent à l'augmentation des rendements. Nos résultats sont également corroborés par Kosma et al. (2022), qui ont comparé les rendements du maïs entre les cultures fertilisées avec des biofertilisants à base d'urine humaine et celles du groupe témoin. Ils ont constaté que le rendement le plus élevé était obtenu avec une application de 0,75 l d'urine humaine par casier, atteignant 5,57 ± 0,50 tonnes par hectare ; en revanche, les plants témoins ont produit le rendement le plus faible avec 2,91 ± 0,45 tonnes par hectare. Ces résultats soulignent l'efficacité des biofertilisants à base d'urine humaine pour améliorer la production de maïs dans les conditions étudiées.

Nos résultats sont également soutenus par une étude utilisant des données provenant de 57 pays en développement montrant que les agriculteurs adoptant des méthodes durables augmentaient leurs rendements en moyenne de 73 % (Pretty & Bharucha, 2014). De plus, une recherche menée par l'ONU en 2008 a révélé une augmentation des rendements agricoles en Afrique de 116 % et de 128 % en Afrique de l'Est par rapport à l'agriculture conventionnelle.

Par ailleurs, l'encadrement agricole et l'accès au crédit jouent un rôle crucial dans la production agricole. Grâce à ces soutiens, les producteurs acquièrent de nouvelles techniques agricoles efficaces qui influencent positivement leurs rendements. Nos résultats s'accordent avec ceux de Kristin et al. (2010), qui affirment qu'en Afrique de l'Est, la formation des agriculteurs via les écoles paysannes a eu un impact positif sur la productivité et le revenu agricole par habitant. L'accès au crédit leur permet également d'investir adéquatement dans l'agriculture grâce à un capital suffisant. En revanche, certaines variables comme MA et COOP dans notre modèle n'ont pas montré d'influence significative sur la production agricole.

5.3 Implication des politiques publiques et l'agroécologie

L'agroécologie présente plusieurs avantages et est souvent perçue comme une voie vers l'atteinte des Objectifs de Développement Durable (ODD). L'agroécologie est un outil pour construire des systèmes alimentaires durables et atteindre les ODD, notamment en éliminant la pauvreté (ODD 1), éradiquant la faim (ODD 2), promouvant la santé (ODD 3), favorisant le travail décent (ODD 8), et luttant contre le changement climatique (ODD 13) (FAO, 2018).

En tant qu'ensemble de pratiques favorisant un développement durable Wezel *et al.*,(2009), elle promeut des modèles de production et de consommation alimentaire plus sains, inclusifs sur le plan social et respectueux des ressources naturelles (Sylvain e*t al*, 2013) . Cependant, le nombre de personnes adoptant ces pratiques est restreint, se limitant principalement à celles qui reçoivent un soutien d'organisations non gouvernementales dans la région de Kirimiro et à travers tout le Burundi. Il existe peu d'incitations issues des politiques publiques pour encourager l'adoption de l'agroécologie, à l'exception de la plantation d'arbres forestiers. Ces observations concordent avec les travaux de Milhorance *et al.,* (2024), qui soulignent que malgré un intérêt croissant pour l'agroécologie en Afrique de l'Ouest, son intégration dans les politiques publiques nationales demeure restreinte, souvent marquée par des compromis fragiles et des objectifs politiques divergents.

La plantation des arbres forestiers et agroforestiers est une pratique assez reconnue et adopté dans notre zone d'étude et partout au Burundi, grâce au programme National appelé, « Ewe Burundi Urambaye » afin de faire face aux changements climatiques à travers la reforestation, l'éducation civique à la protection de l'environnement et l'agroforestier dans les milieux agricoles (MINEAGRIE, 2019). Ces résultats s'alignent à ceux de Bright *et al.,* (2017) qui nous présente divers avantages de l'agroforesterie en démontrant que la présence d'arbustes a augmenté le rendement du mil et de l'arachide de 2011 à 2015. Ils ajoutent également que la présence d'arbustes améliore la qualité du sol.

Le nombre moyen d'arbres agroforestiers plantés par nos répondants au cours des trois dernières années (2022, 2023, 2024) est de 14. Ce chiffre varie de 0 à 60 arbres. La médiane (Me = 10) montre que 50% des ménages interrogés ont planté moins de 10 arbres (la mojorité temoin), tandis que l'autre moitié en a planté plus (groupe I), mais ce chiffre étant pour les arbres agroforestiers seulement.

Bien que l'agroécologie commence à être intégrée dans les politiques africaines, cette intégration reste ambiguë et minoritaire, alors que les politiques agricoles continuent de privilégier une agriculture conventionnelle, axée sur l'augmentation rapide de la production pour lutter contre l'insécurité alimentaire, comme le montre la Politique Nationale de Subvention des engrais chimiques au Burundi (PNSEB). Il est crucial que les stratégies nationales soient développées pour permettre à tous d'adopter ces pratiques agroécologiques.

VI. CONCLUSION

Cette recherche analyse l'impact des pratiques agroécologiques sur la production agricole dans la région de Kirimiro. Des informations ont été recueillies auprès de 252 ménages dans les communes de Giheta et Rutegama, comprenant 125 agriculteurs ayant adopté des pratiques agroécologiques et 127 témoins. Les analyses statistiques ont mis en évidence des différences significatives entre les rendements des agriculteurs utilisant l'agroécologie et ceux qui appliquent des méthodes conventionnelles (témoins). Les résultats d'une régression linéaire multiple indiquent que l'expérience en agroécologie et l'utilisation de biofertilisants sont fortement liées à l'augmentation de la production de maïs. L'accès au crédit et à un encadrement agricole a également un impact positif sur cette production. En outre, l'effet de ces pratiques s'intensifie avec le temps: les agriculteurs ayant plus d'années d'expérience en agroécologie affichent des rendements plus élevés.

RÉFÉRENCES BIBLIOGRAPHIQUES

1. ADISCO (2022). Les pratiques agroécologiques dans la région des grands lacs, 158 p.
2. Ardilly, P. (2006). Les techniques de sondage. Editions Technip.
3. Beillouin, D., Ben-Ari, T., Malezieux, E., Seufert, V. and Makowski, D., (2021). Positive but variable effects of crop diversification on biodiversity and ecosystem services. Global Change Biology. https://onlinelibrary.wiley.com/doi/abs/10.1111/gcb.1574

4. Bergen, D., Contribution à la connaissance des régions naturelles de Burundi; vol 1: Données de superficie et de population par colline de recensement, Bujumbura: ISABU, 1984, 47 p. [Institut des Sciences Agronomiques du Burundi]
5. Bloom, N., & Reenen, J. Van. (2011). Human resource management and productivity. In Handbook of labor economics. Handbook of Labor Economics, 4, 1697–1767. https://www.nber.org/system/files/working_papers/w16019/w16019.pdf
6. Bloom, N., & Reenen, J. Van. (2013b). THE EFFECT OF CLIMATE CHANGE ON GROSS REGIONAL DOMESTIC PRODUCT OF THE AGRICULTURAL SECTOR. NBER Working Paper, XXIII(2), 89.
7. Bright. M. B. H., Diedhiou. I, Bayala. R, Assigbetse. K, Lardy. L. C,Ndour. Y, Dick. R. P, 2017. Long-term Piliostigmareticulatum intercropping in the Sahel: Crop productivity, carbon sequestration, nutrient cycling, and soil quality. Agriculture, Ecosystems and Environment. 9-22
8. Cartier, P. (2022). L' Agroécologie, Pilier d ' une Transition Écologique et Sociale (APTES) au Burundi. 1–23.
9. Chappell, M. J., Bernhart, A., Bachmann, L., Gonçalves, A. L., Seck, S., Nandul, P., Cristo, A., Santos, D., Schneider, S., Dorlöchter-Sulser, S., & Aachen, S. N. (2017). Agroecology as a Pathway towards Sustainable Food Systems. Uniwersytet Śląski,November, 64. https://pureportal.coventry.ac.uk/en/publications/agroecology-as-a-pathway-towards-sustainable- food-systems
10. CNS- FAO, 2016. Working towards Sustainable Agriculture and Food Systems. [on-line]. Available: https://www.blw.admin.ch/dam/blw/en/dokumente/International/Institutionen/CNS%20FAO/Working%20towards%20Sustainable%20Agriculture%20and%20Food%20Systems_discussion%20paper.
11. Dittmer, K. M., Rose, S., Snapp, S. S., Kebede, Y., Brickman, S., Shelton, S., ... & Wollenberg, E. (2023). Agroecology can promote climate change adaptation outcomes without compromising yield in smallholder systems. Environmental Management, 72(2), 333342
12. FAO (2018), FAO's work on agroecology – a pathway to achieving the SDG's.
13. FAO. (2018). Guider La Transition Vers Et Agricoles Durables Les 10 Éléments. FAO, 15.
14. Graziano da Silva J., 2018. Préface. In: Côte F.-X., Poirier-Magona E., Perret S., Rapidel B., Roudier P., Thirion M.-C., eds. *La Transition agro-écologique des agricultures du Sud, Agricultures et défis du monde*, AFD, Cirad, Éditions Quæ, Versailles, 3-4; https://agritrop.cirad. fr/590750/7/ID590750.pdf
15. HLPE. (2019). Approches agroécologiques et autres approches novatrices. Pour une agriculture et des systèmes alimentaires durables propres à améliorer la sécurité alimentaire et la nutrition. Rapport du Groupe d'experts de haut niveau sur la sécurité alimentaire et la nutrition du Comité de la sécurité alimentaire mondiale. 191. http://www.fao.org/cfs/cfs-hlpe/fr/.3 http://www.fao.org/3/i9021en/I9021EN.pdf.
16. ILO (2013) Development: Employment in Africa: Think Agriculture! Disponible sur: https://www.ilo.org/resource/article/employment-africa-think-agriculture consulté le 5/7/ 2024
17. KOUTOU, M. (2023). Agroécologie et entreprenariat, quelles opportunités?: Atelier de formation sur les pratiques agroécologiques avec un accent sur les cultures négligées et sous-utilisées (nus).
18. Kristin, D,, Ephraim, N,, Edward, K,, Daniel, A, M,, Martins, O,, Richard, M,, & Jackson, N, (2010), Impact of Farmer Field Schools on Agricultural Productivity and Poverty in East Africa, IFPRI Discussion Paper 00992,
19. Kuyah, S., Sileshi, G. W., Nkurunziza, L., Chirinda, N., Ndayisaba, P. C., Dimobe, K., & Öborn, I. (2021). Innovative agronomic practices for sustainable intensification in sub-Saharan Africa. A review. *Agronomy for Sustainable Development*, *41*, 1-21.
20. Liu, Y., Ma, X., Shu, L., Hancke, G. P., & Abu-Mahfouz, A. M. (2020). From industry 4.0 to agriculture 4.0: Current status, enabling technologies, and research challenges. IEEE transactions on industrial informatics, 17(6), 4322-4334.

21. Milhorance, C., Sourisseau, J. M., Mané, C. A., Compaoré, E., Piraux, M., Roberto, H. Di, Bayo, F., & Tano, P. K. (2024). L'agroécologie dans les politiques publiques d'Afrique de l'ouest.1–8
22. Ngendakumana S, Minang PA, Feudjio PM, Stijn S, Van Damme P and Tchoundjeu Z (2014). Institutional dimensions of the developing REDD+ process in Cameroon. *Climate Policy Journal*. Vol. 14, No. 4, 1–20, http://dx.doi.org/10.1080/14693062.2014.877221
23. Philippe KOSMA, Ariane Doris JEUTSA, Rosine PATCHONG TCHIMTCHOUA & Mohamadou MOCTAROU YOUSSOUF(2010). Effet du bio fertilisant à base d'urine humaine sur la production de la variété CMS 9015 du maïs (Zea mays L.) dans la localité de Warba, Commune de Mora
24. PNUE-CNUCED.(2008).Agriculture et alimentation biologiques La sécurité en Afrique(Genève: Nations Unies, Genève. Disponible sur http ://tinyurl.com/kcck235, consulté le 14 août 2014
25. Pretty, J. (2007). Agricultural sustainability: concepts, principles and evidence. Philos. Trans. R. Soc. London, Ser. B, 363, 447-465.
26. Pretty, J., & Bharucha, Z. P. (2014). Sustainable intensification in agricultural systems. Annals of Botany, 114(8), 1571–1596. https ://doi.org/10.1093/aob/mcu205
27. Pretty, J., Toulmin, C., & Williams, S. (2011). Sustainable intensification in African agriculture. International Journal of Agricultural Sustainability, 9(1), 5–24. https://doi.org/10.3763/ijas.2010.0583
28. République du Burundi (2023b): Plan National du Développement du Burundi 2018-2027 Révisé et son Plan d'Actions Prioritaires 2023-2027.
29. République du Burundi, MINEAGRIE (2018): Stratégie Agricole Nationale (2018-2027).
30. République du Burundi, MINEAGRIE (2019): Stratégie nationale et plan d'action redd+. burundi.
31. Sylvain Berton, René Billaz, Patrice Burger, A. L. (2013). Agroécologie, une transition vers des modes de vie et de développement viables: Paroles d'acteurs. *Editions Cari 2012, Centre d'actions et de Réalisations Internationales*, 96.
32. Trabelsi, M.(2017). Comment mesurer la performance agroécologique d'une exploitation agricole pour l'accompagner dans son processus de transition? Géographie. Université Paul Valéry – Montpellier III, 2017. Français. FFNNT: 2017 MON30037ff. fftel 01735527
33. Voorn, T. Van Der. (2015). *World Economic and Social Survey 2013 Sustainable Development Challenges* (Issue October).
34. Walpole, M., International, F., & Smith, J. (2013). *Smallholders , food security,. January 2018*.
35. Wezel, A., & Soldat, V. (2009). A quantitative and qualitative historical analysis of the scientific discipline of agroecology. International journal of agricultural sustainability, 7(1), 318.

The Carbon Footprint of Medical Procedures: Drivers, Emissions, and Decarbonization Strategies

Dr. Himanshu Balkumar Gupta

EXECUTIVE SUMMARY

The global healthcare sector, paradoxically, stands as a significant contributor to the very climate crisis it aims to mitigate. Estimates suggest that healthcare accounts for a substantial portion of global greenhouse gas (GHG) emissions, ranging between 4% and 10% of total worldwide emissions, and approximately 8.5% within the United States.[1] This impact directly contradicts the fundamental medical principle of "do no harm," as climate change itself poses a major and escalating threat to human health.

Medical procedures, particularly those conducted within energy-intensive operating rooms (ORs), are identified as primary drivers of these emissions. Key contributors include the disproportionately high energy consumption of ORs, which can be up to six times greater than that of standard clinical wards, the pervasive use of potent Anaesthetic gases, the widespread adoption of single-use medical devices and consumables, and the often-overlooked yet significant carbon footprint associated with patient and staff travel.[3]

Keywords: NA

Classification: LCC Code: RA567

Language: English

Great Britain Journals Press

LJP Copyright ID: 925693
Print ISSN: 2631-8490
Online ISSN: 2631-8504

London Journal of Research in Science: Natural & Formal

Volume 25 | Issue 9 | Compilation 1.0

The Carbon Footprint of Medical Procedures: Drivers, Emissions, and Decarbonization Strategies

Dr. Himanshu Balkumar Gupta

EXECUTIVE SUMMARY

The global healthcare sector, paradoxically, stands as a significant contributor to the very climate crisis it aims to mitigate. Estimates suggest that healthcare accounts for a substantial portion of global greenhouse gas (GHG) emissions, ranging between 4% and 10% of total worldwide emissions, and approximately 8.5% within the United States.[1] This impact directly contradicts the fundamental medical principle of "do no harm," as climate change itself poses a major and escalating threat to human health.

Medical procedures, particularly those conducted within energy-intensive operating rooms (ORs), are identified as primary drivers of these emissions. Key contributors include the disproportionately high energy consumption of ORs, which can be up to six times greater than that of standard clinical wards, the pervasive use of potent Anaesthetic gases, the widespread adoption of single-use medical devices and consumables, and the often-overlooked yet significant carbon footprint associated with patient and staff travel.[3]

Effective strategies for reducing these emissions necessitate a multi-faceted approach. This includes optimizing operational energy use within facilities, transitioning towards reusable medical devices, implementing robust reprocessing programs for single-use devices, adopting Anaesthetic agents with lower global warming potential (GWP), enhancing comprehensive waste management practices, leveraging telehealth services to reduce travel, and integrating sustainable principles into procurement policies. These strategic shifts not only contribute to environmental stewardship but frequently result in considerable economic benefits through cost savings.[8]

Achieving net-zero healthcare demands a systemic transformation, embedding sustainability into every layer of decision-making, from individual clinical actions to overarching national policy frameworks. This report elaborates on these critical drivers and outlines a comprehensive set of strategies to mitigate healthcare's environmental impact.

Author: Director -Administration, Shree Bhagwan Mahaveer Multispecialty Hospital, Chh Sambhajinagar Maharashtra India.

I. INTRODUCTION: THE HEALTHCARE SECTOR'S ENVIRONMENTAL IMPERATIVE

The 21st century recognizes climate change as the foremost global health threat, with its ramifications extending to increased incidences of various diseases, including skin cancers like melanoma, exacerbated by rising ultraviolet radiation due to ozone depletion and global warming.[1] This alarming reality presents a profound paradox: the very systems dedicated to preserving and restoring human health are, through their operational footprint, substantial contributors to this escalating crisis.

The global healthcare sector's carbon footprint is indeed substantial, accounting for approximately 4.4% of global emissions.[2] In the United States, this figure rises to nearly 8.5% of national greenhouse

London Journal of Research in Science: Natural & Formal

gas emissions.[4] To put this into perspective, if the global healthcare system were a sovereign nation, its carbon emissions would rank as the fifth largest worldwide, surpassing even those of Japan.[1] This environmental burden highlights a critical ethical dilemma. The foundational principle of medicine, "primum non nocere" (first, do no harm), extends beyond individual patient care to encompass planetary health. When healthcare operations contribute to environmental degradation that directly harms public health outcomes, a fundamental contradiction arises. Therefore, addressing healthcare's environmental impact is not merely an act of environmental stewardship but a core ethical responsibility, intrinsically linked to the sector's mission to promote and protect health.[7]

Within the broad spectrum of healthcare activities, surgical care and other medical procedures are notably resource-intensive and carbon-heavy areas.[1] Operating rooms (ORs) are consistently identified as major carbon hotspots, consuming three to six times more energy than other clinical areas within a hospital.[5] Furthermore, ORs are prodigious generators of waste, accounting for 50% to 70% of a hospital's total waste output.[8] This report will meticulously examine the specific factors driving emissions within these procedures and delineate actionable strategies for their reduction.

The imperative to address healthcare's carbon footprint is gaining significant traction, reflected in concrete commitments from major health systems globally. The National Health Service (NHS) in the UK, for instance, has pledged to achieve a carbon-neutral service by 2040, with a broader net-zero target by 2045.[1] Similarly, over 1,000 hospitals in the United States have committed to emissions reductions.[2] Despite these growing commitments and increasing awareness among healthcare professionals regarding their sector's environmental impact [15], the actual pace of climate action often falls short of the urgency demanded by the consequences of climate change.[36] This observed gap between recognition and implementation suggests the presence of underlying systemic barriers. These include ingrained arguments of "medical exceptionalism" that propose healthcare should be exempt from decarbonization efforts [37], alongside practical challenges such as a lack of appropriate infrastructure, significant financial considerations, and insufficient education and training for staff.[5] Overcoming these deeply entrenched behavioral and structural challenges will require more forceful, integrated policy interventions and comprehensive educational initiatives to translate awareness into tangible, widespread change.

II. METHODOLOGIES FOR CARBON FOOTPRINTING IN HEALTHCARE

Accurately quantifying environmental impact is a foundational step towards establishing sustainable health systems and facilitating evidence-based policy adjustments.[7] This process is essential for identifying "carbon hotspots" – areas of high emissions – which then become targeted points for intervention.[20] Without precise measurement, efforts to reduce environmental impact may be misdirected or inefficient.

2.1 Life Cycle Assessment (LCA)

Life Cycle Assessment (LCA) stands as an internationally standardized methodology for quantifying the environmental impacts associated with the entire lifecycle of a product, process, or service. Often described as a "cradle-to-grave" approach, LCA meticulously evaluates all stages, from raw material extraction, through manufacturing, transportation, and use, to its eventual disposal.[6] This method systematically measures the energy and materials consumed and the emissions released throughout a defined system.[7] While LCA has been widely adopted and matured in various industries, its application within healthcare is still considered to be in its nascent stages, requiring further research and broader scaling to achieve its full potential.[3] Nevertheless, LCA is an invaluable tool for comparing the environmental impacts of different materials, designs, and processes, such as evaluating the footprint of single-use versus reusable medical products.[38]

2.2 Greenhouse Gas Protocol (Scopes 1, 2, and 3)

The Greenhouse Gas Protocol provides a widely recognized framework for categorizing and reporting carbon emissions, dividing them into three distinct scopes [39]:

- *Scope 1:* These are direct emissions from sources that are owned or controlled by the organization itself. In healthcare, this primarily includes emissions from onsite energy generation and, notably, Anaesthetic gases released during medical procedures.[39]
- *Scope 2:* These represent indirect emissions resulting from the generation of purchased electricity, heating, or cooling consumed by the organization.[39]
- *Scope 3:* This scope encompasses all other indirect emissions that occur within the organization's value chain. For healthcare, this is the most expansive category, covering emissions from the production and transportation of medical devices and pharmaceuticals, waste disposal processes, and the significant impact of patient and staff travel to and from facilities.[9]

A critical observation from current analyses is the overwhelming dominance of Scope 3 emissions in healthcare's total carbon footprint. A majority of healthcare emissions, typically ranging from 50% to 75%, fall under Scope 3, with disposables, equipment, and pharmaceuticals being the largest contributors.[39] This distribution underscores the necessity of a holistic approach to decarbonization that extends far beyond the direct operational boundaries of hospitals.

2.3 Operational vs. Embodied Carbon

Understanding the distinction between operational and embodied carbon is crucial for a comprehensive decarbonization strategy:

- *Operational Carbon:* This refers to the emissions associated with the energy consumed to operate a building or its infrastructure. This includes energy for heating, cooling, ventilation, lighting systems, and the operation of medical equipment.[44] Historically, this has been the primary focus of sustainability initiatives within buildings.
- *Embodied Carbon (also known as Embedded Carbon):* This represents the total greenhouse gases emitted throughout the entire lifecycle of materials and products. This includes emissions from raw material extraction, manufacturing processes, transportation to the site, and even the deconstruction and disposal at the end of a product's useful life.[41] Embodied carbon can constitute a substantial portion, often 20% to 50%, of a product's total life energy.[45] A key characteristic is that, unlike operational carbon emissions which can be reduced through efficiency improvements during use, embodied carbon cannot be reversed once the materials are produced.[45] This makes it a critical consideration for product design and procurement decisions.

The significant contribution of Scope 3 emissions and embodied carbon reveals a substantial environmental burden that often remains less visible than direct operational emissions. The fact that 50% to 75% of healthcare's total emissions are indirect (Scope 3) and that embodied carbon can account for 20% to 50% of a product's total lifecycle emissions means that focusing solely on energy efficiency within hospital buildings, while important, will only address a fraction of the overall problem.[39] This reality implies that genuine decarbonization requires deep engagement with the entire supply chain, including suppliers and manufacturers, to influence product design, material choices, and transportation logistics.

Furthermore, the current state of carbon footprinting in healthcare presents a significant challenge: the application of LCA is described as "in its infancy," and there is a noted "lack of consistency in carbon footprint calculations between studies".[3] This methodological immaturity poses a substantial barrier to effective decarbonization. Without standardized and robust data collection and analytical

methodologies, it becomes difficult to accurately compare the environmental impact of different procedures or products, identify the most impactful hotspots, and reliably measure the effectiveness of interventions. This situation suggests that a foundational step for the healthcare sector must be to invest in developing and mandating consistent carbon footprinting methodologies, potentially through collaborative efforts and regulatory frameworks, to ensure that future sustainability initiatives are truly evidence-based and impactful.

III. KEY DRIVERS OF CARBON EMISSIONS IN MEDICAL PROCEDURES

Medical procedures, particularly those performed in operating rooms (ORs), are inherently resource-intensive and contribute significantly to the healthcare sector's carbon footprint. The primary drivers of these emissions are multifaceted and interconnected.

3.1 Operating Rooms (ORs)

Operating rooms are consistently identified as major carbon hotspots due to their exceptionally high energy intensity and substantial resource consumption. These environments typically consume three to six times more energy per square foot than other clinical wards within a hospital.[5] A predominant portion of this energy consumption, estimated at 90% to 99%, is attributed to heating, ventilation, and air conditioning (HVAC) systems.[14] This energy expenditure is not limited to active use; a significant amount, for instance, two-thirds of yearly CT scanner energy consumption and one-third for MRIs, occurs even when these machines are in idle states.[12]

Beyond energy, ORs are prodigious generators of waste, accounting for 20% to 33% [5] and even up to 50% to 70% [8] of a hospital's total waste. A notable portion of this waste, approximately a quarter, is generated by anesthesia practices alone.[21] Disturbingly, a significant amount of this OR waste is inappropriately segregated, leading to its incineration, a process that itself is carbon-intensive.[5]

The major drivers of emissions within the OR—energy consumption, Anaesthetic gases, and single-use devices—are not isolated issues but are deeply intertwined within the surgical environment. For example, the stringent air exchange rates required for infection control, which necessitate high energy use for HVAC systems, also often contribute to the perceived need for single-use products. Similarly, complex surgical procedures, which typically demand more energy and disposable items, also tend to involve higher usage of potent Anaesthetic gases. This intricate web of interdependencies implies that solutions must be holistic, addressing these connections rather than tackling each component in isolation. A reduction in one area, such as transitioning to reusable items, may necessitate increased energy for sterilization, requiring a systems-thinking approach that considers the full operational and lifecycle impacts.

3.2 Anaesthetic Gases

Volatile Anaesthetic agents are potent greenhouse gases, contributing approximately 5% of a hospital's total carbon emissions.[34] A concerning aspect of their use is that a staggering 95% of inhaled Anaesthetics are not metabolized by the patient but are instead released directly into the atmosphere through the anaesthesia machine's scavenging system.[34] Among these, Desflurane stands out for its exceptionally high global warming potential (GWP); the emissions from a single bottle of Desflurane are equivalent to the carbon footprint of burning 440 kg of coal.[34]

3.3 Medical Devices and Consumables

Medical devices and consumables are consistently identified as the largest contributors to emissions within surgical procedures. The primary carbon hotspot within this category is the material production and manufacturing phase of these items.[3]

The widespread reliance on single-use items, often driven by perceptions of convenience, efficiency, and infection control, significantly inflates the carbon footprint.[8] For instance, a single-use flexible cystoscope generates 2.40 kg of CO2e per procedure, whereas its reusable counterpart accounts for only 0.53 kg of CO2e.[16] This disparity highlights a significant "perception gap" in healthcare. While single-use products are often chosen for perceived ease and safety, evidence demonstrates that reusable alternatives are frequently "environmentally superior and economically advantageous".[11] Moreover, regulated reprocessing of single-use devices (SUDs) has been shown to reduce GHG emissions by 40% to 60% with no increased risk to patient safety.[8] This suggests that a critical barrier to sustainability is not a lack of viable alternatives, but rather a need for robust evidence dissemination and a cultural shift within clinical practice to overcome ingrained habits and misperceptions about safety and cost.

3.4 Medical Imaging and Interventional Procedures

Medical imaging modalities are substantial contributors to healthcare's greenhouse gas emissions. Computed Tomography (CT) and Magnetic Resonance Imaging (MRI) produce considerably more CO2e per examination (6.6 kg and 19.7 kg, respectively) compared to ultrasound (1.2 kg).[12] The increasing demand for diagnostic imaging is projected to lead to a 30% increase in CO2e from CT and MRI by 2030.[12]

Furthermore, the waste generated from contrast agents, such as iodinated media and gadolinium-based contrast agents (GBCAs), poses an environmental concern. These agents have been detected in drinking water, and while clinically stable, GBCAs eventually degrade to free gadolinium, a known environmental toxin.[12] Their indiscriminate disposal is deemed unsustainable.[12] Interventional radiology (IR) procedures also contribute significantly due to their high volume of single-use products, including coils, syringes, wires, and catheters.[12] Studies indicate that climate control systems (HVAC) and disposable surgical items are the largest contributors to IR's carbon footprint.[17]

3.5 Pharmaceuticals

The pharmaceutical industry exhibits a remarkably high carbon intensity, reportedly 55% more carbon intensive than the automotive industry.[2] This makes pharmaceuticals a significant component of healthcare's overall environmental footprint, particularly in specialties like oncology with intensive prescribing practices.[2] The transportation of imported drugs, medical equipment, and supplies further exacerbates these emissions.[2]

3.6 Patient and Staff Travel

Travel associated with healthcare, though often overlooked, contributes substantially to overall emissions. In the United States, patient healthcare-related travel alone generates an estimated 35.7 megatons (Mt) of CO2e annually, accounting for approximately 6% of the nation's total healthcare-related emissions.[10] This impact is particularly pronounced for rural patients, who tend to generate higher emissions per trip due to longer travel distances.[10] Similarly, employee commutes contribute significantly to health system carbon footprints, with annual emissions per participant ranging from 1750 to 3333 kg CO2e in surveyed health systems.[43]

3. 7 Ancillary Services

Even seemingly minor ancillary services contribute to the overall carbon burden. High volume clinical activities such as perioperative group and save (G&S) blood testing have a measurable carbon footprint, calculated at 0.43 kg CO2e for an inpatient sample and 7 kg CO2e for an outpatient sample.

Eliminating unnecessary tests, such as a second G&S in elective cases with low transfusion rates, could save approximately 9 tonnes of CO2e per year.[1] Patient meals also contribute to emissions, estimated at an average of 8.8 kg CO2e per patient-bed-day. Simple dietary changes, such as replacing beef with chicken as a protein source, could reduce these emissions by 29%.[11] Furthermore, laundry processes for hospital linens also add to the carbon footprint, as observed in non melanoma skin cancer surgery, where it accounted for 0.38 kgCO2eq.[13]

3.8 Specialty-Wise Indicative Carbon Emission Data (Per Procedure)

Disclaimer: All figures are approximate and based on current research, often from Western healthcare systems (e.g., UK, USA). Emissions for procedures can vary significantly due to factors mentioned above.

3.9 Tentative Carbon Emissions from Common Medical Procedures: A Tabular Overview

The following table summarizes the indicative carbon dioxide equivalent (CO2e) ranges for common surgical and medical interventions across various specialties, as discussed in the preceding sections. These figures are approximate and subject to variability based on numerous factors, including location, specific hospital practices, and methodology of carbon footprinting.

Specialty	Procedure	Indicative CO2e Range (kg CO2e)
Gynaecology	Laparoscopic Hysterectomy	30-100
Gynaecology	Laparoscopic Ovarian Cystectomy	25-80
Gynaecology	Dilation and Curettage (D&C)	10-30
Gynaecology	Vaginal Delivery	20-50
Gynaecology	C-section	50-150
Gynaecology	Colposcopy/Biopsy (Outpatient)	5-20
Oncology	Mastectomy (with or without lymph node dissection)	70-200
Oncology	Colectomy (Laparoscopic/Open for colorectal cancer)	80-300
Oncology	Lung Resection (e.g., Lobectomy for lung cancer)	100-350
Oncology	Robotic Radical Prostatectomy	40-100

Oncology	Open Radical Prostatectomy	20-70
Oncology	Non-Melanoma Skin Cancer Excision (e.g., Basal Cell Carcinoma)	30-70
General Surgery	Laparoscopic	20-80
	Cholecystectomy	
General Surgery	Appendicectomy (Laparoscopic)	20-70
General Surgery	Laparoscopic Inguinal Hernia Repair	20-70
General Surgery	Open Inguinal Hernia Repair	15-50
General Surgery	Thyroidectomy	30-100
General Surgery	Gastric Bypass/Sleeve Gastrectomy (Bariatric Surgery)	100-300
ENT (Ear, Nose, Throat)	Tonsillectomy/Adenoidectomy (Pediatric)	40-80
ENT (Ear, Nose, Throat)	Myringotomy with Tube Insertion	20-50
ENT (Ear, Nose, Throat)	Septoplasty/Rhinoplasty	50-150
ENT (Ear, Nose, Throat)	Functional Endoscopic Sinus Surgery (FESS)	40-120
ENT (Ear, Nose, Throat)	Cochlear Implant Surgery	100-300
Dentistry including Maxillofacial	Dental Examination/Scale & Polish (Clinic-based)	5-15
Dentistry including Maxillofacial	Dental Filling/Restoration (Clinic-based)	10-30
Dentistry including Maxillofacial	Simple Tooth Extraction (Clinic-based)	10-30

Dentistry including Maxillofacial	Impacted Wisdom Tooth Extraction (OR-based, often GA)	30-80
Dentistry including Maxillofacial	Orthognathic Surgery (Maxillofacial, OR-based)	80-250
Neurosurgery	Craniotomy for Brain Tumor Resection	100-400

Neurosurgery	Spinal Fusion/Disc Surgery	80-300
Neurosurgery	Ventriculoperitoneal (VP) Shunt Insertion	50-150
Neurosurgery	Deep Brain Stimulation (DBS) Surgery	100-350
Neurosurgery	Aneurysm Clipping/Coiling	100-400
Cathlab Procedures (Cardiology/Vascular)	Coronary Angiography/Stenting (PCI)	50-200
Cathlab Procedures (Cardiology/Vascular)	Electrophysiology Study & Ablation (e.g., AF Ablation)	70-300
Cathlab Procedures (Cardiology/Vascular)	Pacemaker/ICD Implantation	30-100
Cathlab Procedures (Cardiology/Vascular)	Peripheral Angiography/Stenting	50-200
Cathlab Procedures (Cardiology/Vascular)	Transcatheter Aortic Valve Implantation (TAVI)	150-500
Urosurgery	Cystoscopy	10-40
Urosurgery	Transurethral Resection of Prostate (TURP)	40-100
Urosurgery	Ureteroscopy (e.g., for stones)	30-100
Urosurg]\ery	Nephrectomy (Laparoscopic/Robotic for kidney cancer)	80-250
Urosurgery	Robotic Radical Prostatectomy	40-100

Urosurgery	Open Radical Prostatectomy	20-70
Interventional Radiology (IR)	Embolization (e.g., UFE, bland embolization)	50-200
Interventional Radiology (IR)	Biopsy (Image-Guided, e.g., Liver/Lung)	20-70
Interventional Radiology (IR)	Drainage Procedures (e.g.,	30-100

	Abscess Drainage)	
Interventional Radiology (IR)	Vertebroplasty/Kyphoplasty	40-120
Interventional Radiology (IR)	Peripheral Artery Intervention	50-200
Other Specialty Major Carbon Emission Rich Procedures	Orthopaedic Surgery - Total Knee Arthroplasty (TKA) / Total Hip Arthroplasty (THA)	80-300
Other Specialty Major Carbon Emission Rich Procedures	Organ Transplantation (e.g., Liver Transplant)	500-1500+
Other Specialty Major Carbon Emission Rich Procedures	Cardiac Surgery (e.g., CABG - Coronary Artery Bypass Grafting)	200-800
Other Specialty Major Carbon Emission Rich Procedures	Plastic Surgery - Major Reconstructive Surgery (e.g., Free Flap)	100-400

3.10 General Notes on Carbon Footprint (CO2e - Carbon Dioxide Equivalent):

Energy: HVAC (heating, ventilation, air conditioning) is a major energy drain.

Anaesthetic Gases: Desflurane and nitrous oxide are potent greenhouse gases.

Consumables/Waste: Single-use instruments, drapes, gowns, and the energy/emissions from their manufacturing, transport, and disposal.

Equipment: Manufacturing and electricity for equipment (cautery, drills, navigation, imaging). Specialty-Wise Indicative Carbon Emission Data (Per Procedure).

Disclaimer: All figures are approximate and based on current research, often from Western healthcare systems (e.g., UK, USA). Emissions for procedures can vary significantly due to factors mentioned above.

3.11 General Takeaways for Reducing Carbon Footprint

Anaesthetic Choices: Prioritize sevoflurane with low flow, propofol, and regional anesthesia over desflurane and nitrous oxide.

Energy Efficiency: Optimize HVAC, lighting, and equipment usage in ORs. Power down equipment when not in use.

Waste Reduction: Reduce single-use plastics and disposables. Explore reprocessing of suitable single-use devices (where safe and regulated). Improve waste segregation and recycling. Sustainable Procurement: Choose suppliers with sustainable practices and products with lower embodied carbon.

Patient and Staff Travel: Promote public transport, carpooling, and telehealth where appropriate. Optimizing Surgical Flow: Shorter, more efficient surgeries reduce energy consumption and consumables.

IV. CARBON REDUCTION STRATEGIES IN MEDICAL PROCEDURES

Mitigating the carbon footprint of medical procedures requires a comprehensive and multi-pronged approach, targeting various aspects of healthcare operations and delivery.

4.1 Operational Efficiency and Energy Management

Optimizing energy consumption within healthcare facilities, particularly in energy intensive areas like operating rooms, is paramount. This involves implementing comprehensive energy audits to identify areas of significant waste and upgrading to more efficient systems. Strategies include enhancing building management systems (BMS) with automated controls that adjust lighting, HVAC, and other systems based on occupancy and real-time energy demand.[24] Reducing air flow turnover in ORs when unoccupied, improving insulation, and installing energy-efficient lighting (e.g., LED) are crucial steps.[11] Initiatives such as the "Operation TLC" (Turn off equipment, Lights out, Control temperatures) implemented by Barts Health NHS Trust, demonstrated significant reductions, saving 2200 tonnes of carbon emissions and £500,000 in energy costs annually.[33]

Beyond structural improvements, equipment management plays a vital role. Implementing "power-down" modes for imaging machines and ensuring that electrosurgical equipment and ventilators are turned off when not in use can yield substantial energy savings.[24] Investing in ENERGY STAR certified medical devices and transitioning to renewable energy sources, such as solar and wind power, either through onsite generation or purchasing green power, further reduces reliance on carbon-intensive grids.[11]

4.2 Sustainable Medical Devices and Consumables

The shift from single-use to reusable medical devices and the reprocessing of single-use devices (SUDs) represent significant opportunities for carbon reduction. Research indicates that switching to reusable instruments can lead to a 38% to 56% reduction in carbon footprint.[22] This applies across various specialties, from general surgery to ENT clinics, where prioritizing reusable metal instruments and optimizing their cleaning in tray sets can enhance efficiency and reduce waste.[11]

Reprocessing SUDs, an FDA-supervised process of cleaning, testing, and repackaging devices for reuse, offers substantial environmental and economic benefits. Studies show a 40% to 60% reduction in GHG emissions when reprocessed devices are used compared to virgin ones.[8] For example, a 49-hospital system partnered with Advantus Health Partners to implement an electrophysiology

equipment reprocessing program, resulting in $4.9 million in savings and preventing over 11,000 pounds of CO2 emissions over four years, all while maintaining high-quality patient care.[26] This directly challenges the perception that sustainable options are inherently costlier or compromise patient safety, as over 25 years of research and regulatory scrutiny have shown no increased risk with reprocessing.[8]

Lean practices and robust waste reduction programs are also essential. This includes optimizing surgical trays to reduce unnecessary instruments, as demonstrated in plastic surgery where redesigned packs saved over €50,000 and 2.9-3.3 tonnes of CO2e annually.[19] Minimizing unnecessary unpacking of instruments in the OR [20] and implementing comprehensive waste segregation and recycling protocols are critical.[5] Adopting circular economy principles, where materials are reused and recycled to the greatest extent possible, transforms waste into a resource, reducing the need for new material extraction.[24]

4.3 Anaesthesia Practices

Anesthesia is a significant contributor to OR emissions, making it a key area for targeted interventions. Choosing inhalational Anaesthetics with lower global warming potential (GWP), such as Sevoflurane over Desflurane, can significantly reduce environmental impact.[11] Furthermore, the adoption of Total Intravenous Anesthesia (TIVA) where appropriate, can reduce the carbon footprint by as much as 20 times compared to inhalation anesthesia.[32] The use of gas purification systems to capture and process Anaesthetic gases before release can also mitigate their environmental impact.[34]

4.4 Optimizing Clinical Pathways

Redesigning care delivery models can improve patient outcomes while simultaneously reducing carbon emissions. A crucial strategy is to reduce low-value care, including eliminating unnecessary procedures and laboratory tests. For instance, rationalizing perioperative group and save (G&S) blood testing by eliminating unnecessary second tests in elective cases could save 9 tonnes of CO2e per year.[1] Similarly, advocating for the judicious use of medical imaging, favoring lower-emission modalities like ultrasound over CT or MRI when clinically appropriate, can significantly reduce emissions.[12]

Shifting care closer to home or into community-based settings, which inherently have a lower carbon footprint than large hospitals, can reduce patient travel and the energy intensity of care delivery.[2] Performing procedures in ambulatory settings, such as using wide-awake local anaesthesia with no tourniquet (WALANT) for hand surgeries, eliminates the need for extensive preoperative tests and anaesthetists, saving both costs and waste (e.g., $13,250 and 2.8 tons of waste over two years in one study).[33]

The increased adoption of telehealth and digital tools, including virtual consultations and remote patient monitoring, offers a powerful means to reduce emissions associated with patient and staff travel. Given that patient travel alone accounts for approximately 35.7 Mt of CO2e annually in the US, expanding telehealth can significantly mitigate this impact, particularly for rural patients who travel longer distances.[2]

4.5 Sustainable Procurement and Supply Chain

Integrating carbon emissions data into procurement decisions is a strategic lever to incentivize suppliers to develop and offer low-carbon medical products.[11] Prioritizing suppliers who demonstrate a commitment to environmental responsibility, possess environmental certifications (e.g., ISO 14001), and source supplies locally can significantly reduce transportation emissions.[24]

Reducing packaging waste is another critical area. This involves choosing packaging made from sustainable, recyclable, or compostable materials and collaborating with suppliers to reduce excessive packaging.[17] The NHS Supply Chain's "Reduce, Reuse, Remanufacture" framework provides practical case studies, such as the introduction of a stand-alone nail pick that reduced single-use plastic, reusable sharps containers that cut 15 tonnes of plastic, and the "Pee in Pot" initiative for sustainable urine testing.[25]

4.6 Innovative Materials and Technologies

Advancements in materials science offer promising avenues for reducing healthcare's environmental impact. The development of cutting-edge biomaterials, biodegradable polymers, and smart substances can revolutionize medical devices, implants, and diagnostics, improving patient outcomes while simultaneously reducing environmental impact.[31] The creation of eco-friendly alternatives, such as plant-based plastics or recyclable components, directly supports the principles of a circular economy, reducing waste and reliance on finite resources.[31]

Sustainable design principles for healthcare facilities also play a crucial role. This includes integrating renewable energy sources (e.g., photovoltaic panels), maximizing natural daylighting, incorporating vegetation and green spaces, implementing rainwater harvesting, and utilizing energy-efficient systems like high-efficiency VRF mechanical systems.[46] Adaptive reuse of existing buildings, rather than new construction, also contributes to reducing embodied carbon and waste.[46]

4.7 Policy and Governance Frameworks

Effective policy and governance are essential to drive systemic change. Establishing national standards and providing financial incentives for low-carbon healthcare operations can standardize efforts and prioritize sustainability initiatives.[11] For instance, the US Inflation Reduction Act offers significant incentives, including a tax credit of up to 30% for installing renewable energy systems and an expanded tax deduction (179D) for energy-efficient commercial buildings, now including nonprofit healthcare facilities.[28] Certification programs, such as The Joint Commission's Sustainable Healthcare Certification for US hospitals, provide a framework for organizations to accelerate decarbonization efforts and gain public recognition for their achievements.[48]

Ultimately, leadership commitment and comprehensive education and training for all healthcare personnel, from clinicians to administrators, are vital to fostering a culture of sustainability.[5] This ensures that sustainability is embedded as a core value and integrated into daily practices and strategic decision-making processes.

V. CONCLUSION AND RECOMMENDATIONS

The analysis unequivocally demonstrates that the healthcare sector carries a significant and paradoxical carbon footprint, contributing substantially to global greenhouse gas emissions despite its mission to heal. This environmental impact is primarily driven by energy-intensive operating rooms, the widespread use of disposable medical devices, potent Anaesthetic gases, and the considerable carbon generated by patient and staff travel. This situation presents a profound ethical challenge, as healthcare's emissions directly undermine public health by exacerbating climate change.

Isolated interventions are insufficient to address this complex challenge. A systemic, multi-faceted approach is imperative, integrating sustainability into every aspect of healthcare delivery and operations. The current landscape also reveals critical methodological gaps, particularly the nascent stage of Life Cycle Assessment application and inconsistencies in carbon footprint calculations across studies, which can hinder effective, evidence-based interventions. Furthermore, a prevailing

"perception gap" regarding the safety and cost-effectiveness of sustainable alternatives, such as reusable devices and reprocessing, acts as a significant barrier to widespread adoption.

Based on this comprehensive review, the following actionable recommendations are proposed to guide the healthcare sector towards a more sustainable and responsible future:

1. Standardize Carbon Foot printing Methodologies: Develop and mandate consistent, robust Life Cycle Assessment (LCA) methodologies across healthcare institutions. This will enable accurate identification of carbon hotspots, allow for reliable comparisons between procedures and products, and provide a clear baseline against which to measure the effectiveness of decarbonization strategies.

2. Prioritize Reusables and Reprocessing: Implement procurement policies that actively favor reusable medical instruments and expand regulated reprocessing programs for single-use devices. This must be supported by comprehensive education and transparent communication to address any lingering concerns about patient safety or cost, leveraging existing evidence that demonstrates both environmental and economic advantages.

3. Optimize Energy Consumption and Anaesthesia Practices: Invest aggressively in energy-efficient infrastructure, including advanced HVAC systems, LED lighting, and smart building management systems. Transition rapidly to renewable energy sources for facility power. Simultaneously, reduce the use of high-GWP Anaesthetic agents, favoring lower-impact alternatives and promoting Total Intravenous Anesthesia (TIVA) where clinically appropriate.

4. Redesign Clinical Pathways for Lower Carbon Footprint: Increase the adoption and accessibility of telehealth services to reduce patient and staff travel. Promote community-based care models and ambulatory surgical settings where feasible. Implement rigorous protocols to reduce low-value care, including unnecessary diagnostic tests and procedures, ensuring that care is both effective and resource efficient.

5. Strengthen Sustainable Procurement and Supply Chain Management: Integrate robust environmental criteria into all purchasing decisions, incentivizing suppliers to develop and provide low-carbon products and services. Foster collaboration with suppliers to reduce excessive packaging and promote circular economy principles throughout the supply chain, emphasizing material reuse and recycling.

6. Foster a Culture of Sustainability through Education: Implement comprehensive, ongoing education and training programs for all healthcare professionals and administrative staff. These programs should raise awareness of healthcare's environmental impact, highlight individual and organizational roles in decarbonization, and equip staff with the knowledge and tools to implement sustainable practices in their daily work.

7. Leverage Policy and Financial Incentives: Advocate for and actively utilize governmental policies, grants, and certification programs designed to support healthcare sustainability initiatives. Engage with policymakers to create frameworks that incentivize decarbonization, such as tax credits for renewable energy adoption and deductions for energy-efficient building upgrades.

Addressing healthcare's carbon footprint is not merely an environmental obligation; it is a critical component of ensuring patient safety, promoting public health, and securing the long-term economic viability of healthcare systems. By embracing these strategies, the sector can uphold its ethical commitment to "do no harm" while leading the way towards a healthier, more sustainable future.

WORKS CITED

1. The carbon footprint of group and save in elective and emergency ..., accessed July 12, 2025, https://publishing.rcseng.ac.uk/doi/10.1308/rcsann.2024.0073
2. Climate change: The problems and potential solutions in oncology - Cancer Control, accessed July 12, 2025, https://www.cancercontrol.info/wp content/uploads/2023/12/12-19-Briggs.pdf
3. The carbon footprint of surgical operations: a systematic review update - ResearchGate, accessed July 12, 2025, https://www.researchgate.net/publication/375180154_The_carbon_footprint_of_sur gical_operations_a_systematic_review_update
4. Cardiac Catheterization Laboratory Sustainability: What it Is and Why it Matters | JACC, accessed July 12, 2025, https://www.jacc.org/doi/10.1016/j.jcin.2023.06.004
5. (PDF) Environmental sustainability in orthopaedic surgery A SCOPING REVIEW, accessed July 12, 2025, https://www.researchgate.net/publication/362701399_Environmental_ sustainability_in_orthopaedic_surgery_a_scoping_review
6. Carbon emission analysis of aortic valve replacement: the environmental footprint of transcatheter vs. surgical procedures - Oxford Academic, accessed July 12, 2025, https://academic.oup.com/eurheartj/advance-articlepdf/doi/10.1093/eurheartj/ehaf379/63640536/ehaf379.pdf
7. About - HealthcareLCA, accessed July 12, 2025, https://healthcarelca.com/background
8. The Case for Hospitals to Boost Single-Use Device Reprocessing Programs - NAM, accessed July 12, 2025, https://nam.edu/perspectives/the-case-for-hospitals-toboost-single-use-device-reprocessing- programs/
9. Confronting Health Care's Carbon Footprint | Harvard Medicine Magazine, accessed July 12, 2025, https://magazine.hms.harvard.edu/articles/confronting-health-cares carbon-footprint
10. Research Spotlight: How Much Does Patient Travel for Healthcare Contribute to Carbon Emissions?, accessed July 12, 2025, https://bwhclinicalandresearchnews.org/2025/03/25/research-spotlight-how much-does-patient-travel-for-healthcare-contribute-to-carbon-emissions/
11. Addressing the environmental impact of healthcare is a vital step to combat the climate crisis, accessed July 12, 2025, https://www.openaccessgovernment.org/article/addressing-the- environmental impact-of-healthcare-is-a-vital-step-to-combat-the-climate-crisis/195152/
12. Environmental sustainability in gynecologic oncology - PMC - PubMed Central, accessed July 12, 2025, https://pmc.ncbi.nlm.nih.gov/articles/PMC11416650/
13. Carbon footprint of non-melanoma skin cancer surgery | BJS Open - Oxford Academic, accessed July 12, 2025, https://academic.oup.com/bjsopen/article/8/5/zrae084/7822229
14. The carbon footprint of products used in five common surgical operations: identifying contributing products and processes - PMC, accessed July 12, 2025, https://pmc.ncbi.nlm.nih.gov/articles/PMC10331364/
15. The Environmental Footprint of Neurosurgery Operations: An Assessment of Waste Streams and the Carbon Footprint - PMC, accessed July 12, 2025, https://pmc.ncbi.nlm.nih.gov/articles/PMC9141268/
16. Carbon footprints in the urologic field: From diagnosis to surgery - PMC - PubMed Central, accessed July 12, 2025, https://pmc.ncbi.nlm.nih.gov/articles/PMC11885924/
17. The Environmental Impact of Interventional Radiology: An Evaluation of Greenhouse Gas Emissions from an Academic Interventional Radiology Practice | Request PDF - ResearchGate, accessed July 12, 2025, https://www.researchgate.net/publication/350464418_The_Environmental_Impact_of_Interventional_Radiology_An_Evaluation_of_Greenhouse_Gas_Emissions_from_an Academic_ Interventional_Radiology_Practice
18. The Environmental Impact of Orthopaedic Surgery - Orthobullets, accessed July 12, 2025, https://upload.orthobullets.com/journalclub/free_pdf/36574633_36574633.pdf
19. Cost-effective strategies for reducing carbon emissions in plastic surgery - PubMed, accessed July 12, 2025, https://pubmed.ncbi.nlm.nih.gov/40578299/

20. What are the main contributors of CO2 emissions in surgery? - SWISS KNIFE, accessed July 12, 2025, https://www.swiss-knife.org/dossiers/innovations/what-arethe-main-contributors-of-co2-emissions-in-surgery
21. Sustainability in the operating room: a cross-sectional survey of nurse anaesthetists' and operating room nurses' views and practice - PMC - PubMed Central, accessed July 12, 2025, https://pmc.ncbi.nlm.nih.gov/articles/PMC12107790/
22. Reducing Environmental Impact in ENT Clinics: Insights from a Literature Review and National Survey on Instrument and Glove Use - ResearchGate, accessed July 12, 2025, https://www.researchgate.net/publication/389494463_Reducing_Environmental_Impact_in_ENT_Clinics_Insights_from_a_Literature_Review_and_National_Survey_on_Instrument_and_Glove_Use
23. pmc.ncbi.nlm.nih.gov, accessed July 12, 2025, https://pmc.ncbi.%20devices%20generates,0.53%20kg%20of%20CO2.&text=Using%20disposable%20drapes%20and%20gowns,by%20switching%20to%20reusable%20items.
24. Strategies for Healthcare Organizations to Mitigate Supply Chain Carbon Footprints and Enhance Sustainability Efforts | Simbo AI - Blogs, accessed July 12, 2025, https://www.simbo.ai/blog/strategies-for-healthcare-organizations-to-mitigatesupply-chain-carbon-footprints-and-enhance-sustainability-efforts-188537/
25. Sustainable Actions - NHS Supply Chain, accessed July 12, 2025, https://www.supplychain.nhs.uk/programmes/sustainability/case-studies/
26. Here's How One Health System Saved Millions by Reprocessing ..., accessed July 12, 2025, https://advantushp.com/news/heres-how-one-health-system-saved-millionsby-reprocessing-medical-devices/
27. Healthcare Carbon Reduction Strategies → Term - Energy → Sustainability Directory, accessed July 12, 2025, https://energy.sustainability-directory.com/term/healthcare-carbon-reduction-strategies/
28. Funding health care sustainability initiatives | HFM Magazine, accessed July 12, 2025, https://www.hfmmagazine.com/funding-sustainability-initiatives-health-care
29. Lowering Carbon Emissions Through Redesigned Health Care ..., accessed July 12, 2025, https://www.commonwealthfund.org/blog/2023/lowering-carbon-emissionsthrough-redesigned-health-care
30. The potential of virtual healthcare technologies to reduce healthcare services' carbon footprint - PMC, accessed July 12, 2025, https://pmc.ncbi.nlm.nih.gov/articles/PMC11137209/
31. www.medtecheurope.org, accessed July 12, 2025, https://www.medtecheurope.org/environmental-and-socialsustainability/sustainable-materials-and-substanceinnovation/#:~: text=Cutting%2Dedge%20biomaterials%2C%20biodegradable%20polymers,outcomes%20while%20reducing%20environmental%20impact.
32. Sustainable Surgery Alternatives | Tunley Environmental, accessed July 12, 2025, https://www.tunley- environmental.com/en/insights/sustainable-surgery-alternatives
33. Carbon Neutral Hand Surgery: Simple Changes to Reduce Carbon Footprint - PMC, accessed July 12, 2025, https://pmc.ncbi.nlm.nih.gov/articles/PMC10902490/
34. Carbon Footprint and Sustainability in The Operating Room: What to Know on the Road to Becoming a Green Operating Room - ResearchGate, accessed July 12, 2025, https://www.researchgate.net/publication/392175954_Carbon_Footprint_and_Sustainability_in_The_Operating_Room_What_to_Know_on_the_Road_to_Becoming_a_Green_Operating_Room
35. Carbon Emissions From Patient Travel for Health Care - PMC - PubMed Central, accessed July 12, 2025, https://pmc.ncbi.nlm.nih.gov/articles/PMC11959441/

36. Twelve actions in healthcare to reduce carbon emissions | European Journal of Cardiovascular Nursing | Oxford Academic, accessed July 12, 2025, https://academic.oup.com/eurjcn/ article/23/ 1/e6/7236421
37. Who Carries the Responsibility for Health Care Carbon Reduction? - PMC, accessed July 12, 2025, https://pmc.ncbi.nlm.nih.gov/articles/PMC12207287/
38. Introduction - Use of Life Cycle Assessment in the Healthcare Industry: Environmental Impacts and Emissions Associated With Products, Processes, and Waste - NCBI, accessed July 12, 2025, https://www.ncbi.nlm.nih.gov/sites/books/NBK610175/?report=reader
39. The carbon footprint of healthcare settings: A systematic review - PubMed, accessed July 12, 2025, https://pubmed.ncbi.nlm.nih.gov/37198974/
40. Carbon emission analysis of aortic valve replacement: the environmental footprint of transcatheter vs. surgical procedures | European Heart Journal | Oxford Academic, accessed July 12, 2025, https://academic.oup.com/eurheartj/advance-articleabstract/doi/10.1093/eurheartj/ehaf379/818 1057
41. Embodied Carbon (Embedded Carbon) - The Chancery Lane Project, accessed July 12, 2025, https://chancerylaneproject.org/glossary/embodied-carbon-embedded carbon/
42. pubmed.ncbi.nlm.nih.gov, accessed July 12, 2025, https://pubmed.ncbi.nlm.nih.gov/ 37198974/#:~:text=The%20Greenhouse%20Gas%20Protocol%20divides,environmental%20impac t%20of%20health%20services.
43. The Carbon Footprint of Health System Employee Commutes - ResearchGate, accessed July 12, 2025, https://www.researchgate.net/publication/368359664_The_Carbon_Footprint_of_Health _System_Employee_Commutes
44. Operational & Embodied Carbon | UKGBC, accessed July 12, 2025, https://ukgbc.org/wp-content/uploads/2023/02/operational-and-embodied carbon-1.pdf
45. Understanding Embodied Carbon - Midas Pattern, accessed July 12, 2025, https://www.Midas-pattern.co.uk/news/understanding-embodied-carbon
46. 16 Sustainable Health Care Design Examples - gb&d magazine, accessed July 12, 2025, https://gbdmagazine.com/ sustainable-health-care-design-examples/
47. Sustainable materials and substance innovation - MedTech Europe, accessed July 12, 2025, https://www.medtecheurope.org/environmental-and-socialsustainability/sustainable-materials-and-substance-innovation/
48. Sustainable Healthcare | The Joint Commission, accessed July 12, 2025, https://www. jointcommission. org/resources/sustainable-healthcare/

Discrete Maximum Principle Honored by Nite Volume Schemes for Diusion-Convection- Reaction Problems Proof with Geometrical Arguments

Abdou Njifenjou

ABSTRACT

From the Engineering point of view, the Maximum Principle is physically an important property met by solutions of elliptic partial differential equations (PDE for short) of second order governing di sion-convection- reaction phenomena. This property is also called Positivity-Preserving Property in the literature. At the discrete level the Positivity-Preserving Property is required for any numerical scheme designed for solving such PDE. By means of algebraic arguments it is well-known that conventional nite volume schemes for second order elliptic PDE meet the discrete maximum principle. In this communication we expose a new technique based upon geometric arguments for proving that conventional nite volume schemes for di usion-convection-reaction problems meet the discrete version of Maximum Principle. Notice that the above mentioned geometrical technique works for any space dimension.

Keywords: discrete maximum principle, geometric arguments, diffusion-adjection-reaction problems, nite volume schemes.

Classification: LCC Code: QA377

Language: English

Great Britain Journals Press

LJP Copyright ID: 925694
Print ISSN: 2631-8490
Online ISSN: 2631-8504

London Journal of Research in Science: Natural & Formal

Volume 25 | Issue 9 | Compilation 1.0

Discrete Maximum Principle Honored by Nite Volume Schemes for Diusion-Convection-Reaction Problems Proof with Geometrical Arguments

Abdou Njifenjou

ABSTRACT

From the Engineering point of view, the Maximum Principle is physically an important property met by solutions of elliptic partial differential equations (PDE for short) of second order governing di sion-convection- reaction phenomena. This property is also called Positivity-Preserving Property in the literature. At the discrete level the Positivity-Preserving Property is required for any numerical scheme designed for solving such PDE. By means of algebraic arguments it is well-known that conventional nite volume schemes for second order elliptic PDE meet the discrete maximum principle. In this communication we expose a new technique based upon geometric arguments for proving that conventional nite volume schemes for di usion-convection-reaction problems meet the discrete version of Maximum Principle. Notice that the above mentioned geometrical technique works for any space dimension.

Keywords: discrete maximum principle, geometric arguments, diffusion-adjection-reaction problems, nite volume schemes.

I. INTRODUCTION

Let Ω be a bounded connected open subset of $\mathbb{R}^2$ whose boundary denoted by Γ is the union of polygonal lines $\Gamma_k]_{k\in K}$ where K is a finite subset of $\mathbb{N}$ which denotes the set of positive integers (see Figure 1 below). Note that if K is a singleton then Ω is a polygon (and so simply connected). Given the scalar functions $D(\cdot)$, $\mu(\cdot)$ and $f(\cdot)$ together with a vector field $(\cdot)$, all being defined in Ω, we consider the elliptic problem that consists in finding a scalar function $u(.)$ in an adequate function space such that

$$-\,div\,[D(x)grad\,u]\,+\,div\,[u\,\psi]\,+\,\mu\,u\quad=\quad f\quad\text{in}\quad\Omega \tag{1.1}$$

with the following homogeneous Dirichlet boundary conditions :

$$u\,=\,0\qquad\text{on}\qquad\Gamma \tag{1.2}$$

Under reasonable assumptions on the previous data i.e.

$$0<D^{-}\,\leq\,D(x)\,\leq\,D^{+},\quad and\quad \mu(x)\geq 0\quad a.e.\ in\ \Omega \tag{1.3}$$

London Journal of Research in Science: Natural & Formal

$$f(\cdot) \in L^2 \ \ (\Omega) \tag{1.4}$$

$$\psi(.) \in C^1(\overline{\Omega}, \mathbb{R}^2 \ \ ) \tag{1.5}$$

with

$$div\,[\psi] \ \geq \ 0 \quad a.e.\ in\ \Omega \tag{1.6}$$

it is easy to prove that (see [1] for instance): The second order elliptic problem (1.1)-(1.2) gets a unique weak solution in the sense that

$$(PV) \quad \begin{cases} \text{There exists one and only one } \ u \in H_0^1(\Omega) \text{ such that :} \\ \mathcal{B}(u,v) \ = \ L(v) \qquad \forall v \in H_0^1(\Omega) \end{cases} \tag{1.7}$$

where we have set:

$$\mathcal{B}(u,v) = \int_\Omega D(x) grad\, u.grad\, v\, dx \ + \ \int_\Omega v\, div\,[u\,\psi]\, dx \ + \ \int_\Omega \mu\, u\, v\, dx \tag{1.8}$$

and

$$L(v) = \int_\Omega f\, v\, dx. \tag{1.9}$$

Following [2] one can prove that if the given function f is positive almost everywhere in Ω then the weak solution of the system (1.1)-(1.2) is also positive almost everywhere in Ω. That is the weak form of the Maximum Principle. Several works on construction of positivity-preserving numerical methods for diffusion, diffusion-convection, diffusion-reaction and diffusion-convection-reaction problems are available in the literature (see for instance [5, 6, 11, 13]). Such numerical methods are sometimes called monotone schemes.

The main objective of this work is to expose geometrical arguments for proving the well-known discrete version of the Maximum Principle satisfied by the conventional finite volume solution to the system (1.1)-(1.2).

II. PRELIMINARY TOOLS

Definition 2.1 (Partition of Ω). Let $\overline{\Omega}$ be the closure of Ω in the sense of the standard topology of $\mathbb{R}^2$ and let J be a finite subset of $\mathbb{N}$ which is the set of positive integers. A family $\{\Omega_j\}_{j\in J}$ made up of subsets of $\overline{\Omega}$ defines a partition of $\overline{\Omega}$ if the following conditions are satisfied:

$$\begin{cases} (i) \quad Int(\Omega_j) \neq \emptyset \qquad \forall j \in J \\ (ii) \quad \overline{\Omega} = \underset{j\in J}{\cup} \overline{\Omega}_j \\ (iii) \quad \forall j', j'' \in J, \qquad j' \neq j'' \implies Int(\Omega_{j'}) \cap Int(\Omega_{j''}) \ = \ \emptyset \end{cases} \tag{2.1}$$

where $Int(\diamond)$ denotes the interior of $\diamond$ in the sense of standard topology of $\mathbb{R}^2$.

Let us consider a *partition* $\mathcal{P}$ over Ω consisting in a finite family of closed convex polygons (named also polygonal elements) generically denoted by T. These polygonal elements are the so-called control volumes in the language of Finite Volume theory. The control volumes from the partition $\mathcal{P}$ defines a *conforming Finite Volume mesh* over $\overline{\Omega}$ if (in addition to conditions (i)-(iii) from Definition 2.1) the following conditions are satisfied:

$$\begin{cases} \forall T', T'' \in \mathcal{P}, \qquad T' \neq T'' \ \text{ implies that :} \\ \circ \quad \text{either} \quad T' \cap T'' = \emptyset \\ \circ \quad \text{or} \quad T' \cap T'' = \text{ common vertex} \\ \circ \quad \text{or} \quad T' \cap T'' = \text{ common edge,} \end{cases} \tag{2.2}$$

where $\emptyset$ denotes the empty set. Let us denote by $\partial\mathcal{P}$ the set of boundary edges (viewed as degenerate control volumes) and we briefly define the conventional finite volume mesh $\mathcal{T}$ as it follows: $\mathcal{T} = \{\mathcal{P}, \partial\mathcal{P}\}$.

We should use intensively in what follows a notion of characteristic function slightly different from the usual one and defined as follows.

Definition 2.2 Let T be a control volume either from $\mathcal{P}$ or from $\partial\mathcal{P}$. We call in this work the characteristic function of T denoted by $\mathbf{1}_T$ the function defined almost everywhere either in Ω (with respect to Lebesgue measure in 2-D) or on $\Gamma = \underset{k\in K}{\cup} \Gamma_k$ (with respect to Lebesgue measure in 1-D) by :

$$\mathbf{1}_T(x) = \begin{cases} 1 & \text{if} \quad x \in Int(T) \\ 0 & \text{if} \quad x \in Ext(T) \end{cases} \tag{2.3}$$

where $Ext(\diamond)$ denotes the exterior of a subset $\diamond$ from $\mathbb{R}^2$ (with respect to the natural topology of $\mathbb{R}^2$). Recall that $Int(\diamond)$ stands for the interior of $\diamond$ from $\mathbb{R}^2$. $\square$

Let us introduce the following discrete function spaces that play a key-role in the sequel.

Definition 2.3 We set :

$$\mathbf{S}^{\mathcal{P}} = \Big\{ v_{\mathcal{P}} : \Omega \longrightarrow \mathbb{R} \,;\, v_{\mathcal{P}}(x) = \sum_{T\in\mathcal{P}} v_T \mathbf{1}_T(x), \ \text{with } v_T \in \mathbb{R} \ \ \forall T \in \mathcal{P} \Big\}, \tag{2.4}$$

$$\mathbf{S}^{\partial\mathcal{P}} = \Big\{ v_{\partial\mathcal{P}} : \Gamma \longrightarrow \mathbb{R} \,;\, v_{\partial\mathcal{P}}(s) = \sum_{L\in\partial\mathcal{P}} v_L \mathbf{1}_L(s), \ \text{with } v_L \in \mathbb{R} \ \ \forall L \in \partial\mathcal{P} \Big\}, \tag{2.5}$$

and

$$\mathbf{S}^{\mathcal{T}} = \mathbf{S}^{\mathcal{P}} \times \mathbf{S}^{\partial\mathcal{P}}, \qquad \mathbf{S}_0^{\mathcal{T}} = \mathbf{S}^{\mathcal{P}} \times \Big\{ 0_{\mathbf{S}^{\partial\mathcal{P}}} \Big\} \tag{2.6}$$

where $0_{\mathbf{S}^{\partial\mathcal{P}}}$ is the zero-function (denoted simply 0 if there is no risk of confusion) from the discrete function space $\mathbf{S}^{\partial\mathcal{P}}$. $\square$

The Finite Volume method is based on the fundamental idea that the exact solution u could be approximated inside any control-volume T with a constant U_T corresponding to either the mean-value of u or its approximation at a given point located inside T, with Cartesian coordinates x_T. In the context of conventional Finite Volumes the choice of that point is not arbitrary as we will be seeing in assumption $(\mathcal{A}_3)$ below. Let us denote by Γ_T the boundary of any control-volume T. We need to specify the following assumptions that make the conventional Finite Volumes very attractive and realistic for certain engineering problems as subsurface flow problems (notice that [3, 4, 15] are among distinguished references on fluid flow in porous media):

$(\mathcal{A}_1)$ The diffusion coefficient $D(\cdot)$ is a piecewise constant function i.e.

$$\exists\, S \subseteq \mathbb{N}, \text{ with } S \text{ finite, such that:} \qquad D(x) = \sum_{s\in S} D_s \mathbf{1}_{\Omega_s}(x). \tag{3.1}$$

where $\{\Omega_s\}_{s\in S}$ defines a partition $\mathcal{P}$ of the domain $\overline{\Omega}$ in the sense of Definition 2.1.

Denote by $\mathcal{T}$ the Finite Volume mesh corresponding to the partition $\mathcal{P}$. Let us make the following assumption on $\mathcal{T}$.

$(\mathcal{A}_2)$ $\mathcal{T}$ is compatible with the discontinuities of $D(\cdot)$ in the sense that the discontinuity points of $D(\cdot)$ belong to the mesh interfaces $\Gamma^{\mathcal{T}} = \underset{T\in\overline{\mathcal{P}}}{\cup} \Gamma_T$, where we have set $\overline{\mathcal{P}} = \mathcal{P} \cup \partial\mathcal{P}$. In other words any discontinuity point of the function $D(\cdot)$ is located in a control volume boundary.

$(\mathcal{A}_3)$ For all $(T', T'') \in \overline{\mathcal{P}} \times \mathcal{P}$ such that T' and T'' are adjacent (that is $\Gamma_{T'} \cap \Gamma_{T''}$ is a common edge for control volumes T' and T''), the vector $x_{T'} - x_{T''}$ is orthogonal to the common edge. This is the so-called orthogonality condition required for conventional Finite Volume meshes (see [5, 6]).

An immediate consequence of the assumption (1.3) is that $D(\cdot)$ is a nonnegative constant function in each control volume T. We denote by D^T the constant value of $D(\cdot)$ in the control volume T.

Let us give a brief description of the different steps for getting a conventional finite volume scheme. We start with introducing some useful notations: $\mathcal{E}$ is the set of all mesh edges, $\mathcal{E}^{int}$ is the subset of $\mathcal{E}$ made of interior mesh edges and $\mathcal{E}^{ext}$ is the subset of $\mathcal{E}$ made of exterior mesh edges i.e. mesh edges lying on the domain boundary.

Step 1: Integrate the two sides of the balance equation (1.1) in each control volume T from the family $\mathcal{P}$. So we get what follows (thanks to Ostrogradski's theorem):

$$-\int_{\Gamma_T} D^T grad\, u \,.\, \nu_T ds + \int_{\Gamma_T} u\,\psi \,.\, \nu_T ds + \int_T \mu(x)u(x)dx = \int_T f(x)dx \qquad \forall\, T \in \mathcal{P}. \tag{3.2}$$

where ν_T stands for outward unit vector normal to the control-volume boundary Γ_T.

Step 2 : Re-write the first two integral terms from the left-hand side of (3.2) as follows for all $T \in \mathcal{P}$:

$$\sum_{\sigma \in \mathcal{E}_T} -\int_{\sigma} D^T grad\, u \,.\, \nu_{\sigma,T} ds \;+\; \sum_{\sigma \in \mathcal{E}_T} \int_{\sigma} u\, \psi \,.\, \nu_{\sigma,T} ds \;+\; \int_T \mu(x) u(x) dx \;=\; \int_T f(x) dx \tag{3.3}$$

where $\mathcal{E}_T$ is the set of mesh edges σ lying in Γ_T and where $\nu_{\sigma,T}$ stands for outward unit vector normal to the portion σ of the control-volume boundary Γ_T, called again mesh edge associated with Γ_T. Integrals from the first summation are diffusion fluxes while integrals from the second summation are convection fluxes (called sometimes advection fluxes).

Step 3: Perform the approximation of the unknown function u in the control-volume T with the unknown real constant $u(x_T)$. So one could set what follows concerning approximation of the reaction term :

$$\int_T \mu(x) u(x) dx \;\approx\; u(x_T)\, I_T(\mu) \qquad \forall T \in \mathcal{P} \tag{3.4}$$

where $I_T(\diamond)$ is the integral of a function $\diamond$ defined in the control volume T.

Step 4 : Look for reasonable approximations of flux integral terms from the left-hand side of (3.3). What should one understand by reasonable approximations ? We mean that the flux approximations should take account of the following constraints :

• Perform the upwind approximation of the convection flux in view to ensure the stability of the global finite volume scheme. For that purpose, let us start with setting :

Definition 3.1

$$\psi_{\sigma,T} \;\stackrel{def}{=}\; \int_{\sigma} \psi \,.\, \nu_{\sigma,T} ds \tag{3.5}$$

Definition 3.2 (Upwind approximation of the convection flux over $\sigma \in \mathcal{E}^{int}$)
Let σ in $\mathcal{E}_T \cap \mathcal{E}_L$, with T and L from the set $\mathcal{P}$. We set:

$$\int_{\sigma} u\, \psi \,.\, \nu_{\sigma,T} ds \;\approx\; \begin{cases} u(x_T)\, \psi_{\sigma,T} & \text{if} \quad \psi_{\sigma,T} \geq 0 \\ u(x_L)\, \psi_{\sigma,T} & \text{if} \quad \psi_{\sigma,T} < 0. \end{cases} \tag{3.6}$$

In other words the upwind approximation of the convective flux across the interior edge σ in $\mathcal{E}_T \cap \mathcal{E}_L$ could be defined as follows :

$$\int_{\sigma} u\, \psi \,.\, \nu_{\sigma,T} ds \;\approx\; u(x_T)\, \max\{\psi_{\sigma,T}, 0\} \;-\; u(x_L)\, \max\{-\psi_{\sigma,T}, 0\}. \tag{3.7}$$

Since (according to the flux continuity principle over grid-block interfaces)

$$\psi_{\sigma,T} \;+\; \psi_{\sigma,L} \;=\; 0$$

the preceding approximation of the convective flux is equivalent to the following one

$$\int_\sigma u\,\psi\,.\,\nu_{\sigma,T}ds \approx u(x_T)\,\max\{\psi_{\sigma,T},0\} - u(x_L)\,\max\{\psi_{\sigma,L},0\}. \tag{3.8}$$

• The flux continuity across interior edges σ, i.e. $\sigma \in \mathcal{E}^{int}$, is a fundamental physical principle to be met. So we have necessarily for all $\sigma \in \mathcal{E}^{int}$

$$[-D^T grad\,u\,.\,\nu_{\sigma,T} + u\,\psi\,.\,\nu_{\sigma,T}] +$$

$$+ [-D^L grad\,u\,.\,\nu_{\sigma,L} + u\,\psi\,.\,\nu_{\sigma,L}] = 0 \qquad on \quad \sigma \tag{3.9}$$

Integrating the right-hand and the left-hand sides of (3.9) over $\sigma \in \mathcal{E}^{int}$ leads to the following "weak formulation" of flux continuity :

$$[-\int_\sigma D^T grad\,u\,.\,\nu_{\sigma,T}ds + \int_\sigma u\,\psi\,.\,\nu_{\sigma,T}ds] +$$

$$+[-\int_\sigma D^L grad\,u\,.\,\nu_{\sigma,L}ds + \int_\sigma u\,\psi\,.\,\nu_{\sigma,L}ds] = 0 \qquad \forall\,\mathcal{E}^{int} \ni \sigma = \Gamma_T \cap \Gamma_L \tag{3.10}$$

Since the weak solution u of the system (1.1)-(1.2) lies in $H_0^1(\Omega)$, the trace $u_{|_\sigma}$ exists (in $H^{\frac{1}{2}}(\sigma)$ for instance) in a unique manner. In consequence we naturally get what follows :

$$[\int_\sigma u\,\psi\,.\,\nu_{\sigma,T}ds] + [\int_\sigma u\,\psi\,.\,\nu_{\sigma,L}ds] = 0 \qquad \forall\,\mathcal{E}^{int} \ni \sigma = \Gamma_T \cap \Gamma_L \tag{3.11}$$

Thus, the previous "weak formulation" of flux continuity (3.10) is reduced to

$$[-\int_\sigma D^T grad\,u\,.\,\nu_{\sigma,T}ds] + [-\int_\sigma D^L grad\,u\,.\,\nu_{\sigma,L}ds] = 0 \qquad \forall\,\mathcal{E}^{int} \ni \sigma = \Gamma_T \cap \Gamma_L \tag{3.12}$$

In the context of conventional Finite Volumes the family $\mathcal{P}$ satisfies the so-called orthogonality condition (see assumption $(\mathcal{A}_3)$ above at the beginning of the current Section). So there exists a family of points $\{x_T;\ T \in \mathcal{P}\}$, such that for any pair $(T,L) \in \mathcal{P} \times \overline{\mathcal{P}}$, with T and L adjacent, the orthogonal projections of x_T and x_L on their common edge σ coincides and let call it x_σ. We make the following convention:

"If T is adjacent to the domain boundary we set : $L \stackrel{def}{=} \sigma$, where σ is the boundary edge associated with T, and x_L coincides with x_σ".

This being said, from the following diffusion flux approximation (assuming the exact solution restriction $u_{|_T}$ in $C^0(\overline{T})$ for any $T \in \mathcal{P}$; it is the case if $u_{|_T} \in H^2(T)$):

$$-\int_{\sigma}[D^T grad\, u\ .\ \nu_{\sigma,T}]ds\ \approx\ \frac{D^T\, mes(\sigma)}{dist(x_T, x_\sigma)}[u(x_T) - u(x_{\sigma,T})] \qquad \forall\, \sigma \in \mathcal{E}_T \qquad (3.13)$$

where $mes(\,.\,)$ stands for Lebesgue measure in one-space dimension, $dist(.,.)$ represents the Euclidean distance and where $x_{\sigma,T}$ is in fact the point x_σ seen as from the boundary of T by an observer standing inside T. The principle of continuity of u on grid-block interfaces is expressed at the discrete level by the relation :

$$u(x_{\sigma,T})\ =\ u(x_{\sigma,L}) \qquad \forall\, \sigma \in \mathcal{E}_T \cap \mathcal{E}_L \qquad \forall\, T, L \in (\mathcal{P} \times \mathcal{P})_{adj}$$

where $(\mathcal{P} \times \mathcal{P})_{adj}$ is the subset of $\mathcal{P} \times \mathcal{P}$ made of (T, L) such that T and L are adjacent. So it is reasonable to set:

$$u(x_\sigma) \stackrel{def}{=} u(x_{\sigma,T}) \qquad \forall\, T \in \mathcal{P} \qquad \forall\, \sigma \in \mathcal{E}_T.$$

With the above notation the diffusion flux approximation could read as follows

$$-\int_{\sigma}[D^T grad\, u\ .\ \nu_{\sigma,T}]ds\ \approx\ \frac{D^T\, mes(\sigma)}{dist(x_T, x_\sigma)}[u(x_T) - u(x_\sigma)] \qquad \forall\, \sigma \in \mathcal{E}_T \qquad (3.14)$$

Writing down the *discrete analogue* of the "weak formulation" (3.12) of continuity of the diffusion flux (across any interior edge $\sigma \in \mathcal{E}_T \cap \mathcal{E}_L$) yields

$$\frac{D^T\, mes(\sigma)}{dist(x_T, x_\sigma)}[u(x_T) - u(x_\sigma)]\ +\ \frac{D^L\, mes(\sigma)}{dist(x_L, x_\sigma)}[u(x_L) - u(x_\sigma)] = 0 \qquad \forall\, \sigma \in \mathcal{E}_T \cap \mathcal{E}_L. \qquad (3.15)$$

This relation could be viewed as a linear equation with only discrete unknown $u(x_\sigma)$. This unknown can be obviously determined as a function of discrete unknowns $u(x_T)$ and $u(x_L)$ as indicated hereafter. Indeed elementary operations on (3.15) leads to

$$u(x_\sigma)\ =\ \frac{\lambda_{T,\sigma}\, u(x_T)\ +\ \lambda_{L,\sigma}\, u(x_L)}{\lambda_{T,\sigma}\ +\ \lambda_{L,\sigma}} \qquad \forall\, \sigma \in \mathcal{E}_T \cap \mathcal{E}_L \qquad (3.16)$$

where we have set

$$\lambda_{K,\sigma} \stackrel{def}{=} \frac{D^K}{dist(x_K, x_\sigma)} \qquad \forall\, K \in \mathcal{P} \qquad \forall\, \sigma \in \mathcal{E}_K. \qquad (3.17)$$

Substituting the right-hand side of (3.16) to $u(x_\sigma)$ in the diffusion flux approximation given by (3.14) leads to what follows for any $\sigma \in \mathcal{E}_T \cap \mathcal{E}_L$:

$$-\int_{\sigma}[D^T grad\, u\ .\ \nu_{\sigma,T}]ds\ \approx\ \frac{D^T D^L mes(\sigma)}{D^T dist(x_L, x_\sigma) + D^L dist(x_T, x_\sigma)}[u(x_T) - u(x_L)]\,. \qquad (3.18)$$

Remark 3.3 (Important to notice)

First of all the diffusion flux approximation (3.18) has been established for interior edges i.e. $\sigma \in \mathcal{E}^{int}$. Let us explain why the convention consisting to consider boundary edges σ as also degenerate control-volumes L allows to recover (3.14) from the relation (3.18). Indeed if $\sigma \in \mathcal{E}_T \cap \mathcal{E}^{ext}$ then $x_\sigma = x_L$, and it follows that $dist(x_L, x_\sigma) = 0$ in (3.18).

The following Conventional Finite Volume scheme is obtained from preceding approximations of different terms of the left-hand side of the balance equation (3.3): see relations (3.4), (3.8) and (3.18). One could learn more on this topic with [5, 6] for instance.

Definition 3.4 (Conventional Finite Volume Scheme)

The conventional Finite Volume approximation of the system (1.1)-(1.2) consists in what follows :

Find

$$U_{\mathcal{T}} = (\sum_{K\in\mathcal{P}} U_K \mathbf{1}_K \, , \, 0_{\mathbf{S}^{\partial\mathcal{P}}}) \in \mathbf{S}_0^{\mathcal{T}}$$

such that:

$$\sum_{L\in\overline{\mathcal{P}},L\neq T} \frac{D^T D^L mes(\Gamma_T \cap \Gamma_L)}{D^T dist(x_L,T) + D^L dist(x_T,L)}[U_T - U_L] +$$

$$+ \sum_{L\in\overline{\mathcal{P}},L\neq T} [U_T \max\{\psi_{\sigma,T}, 0\} - U_L \max\{\psi_{\sigma,L}, 0\}] + U_T \, I_T(\mu) = I_T(f) \quad \forall T \in \mathcal{P} \tag{3.19}$$

where $\sigma \in \mathcal{E}_T \cap \mathcal{E}_L$. Recall that $I_T(\diamond)$ is the integral of a function $\diamond$ defined in the control volume T. □

The Finite Volume and Mimetic Finite Difference approximations of solutions to isotropic or anisotropic diffusion problems on distorted grids have been intensively developed in the literature and are today considered as classical topics (see for instance [6, 7, 8, 9, 10, 14]. Some extensions of Finite Volume Methods have been designed and known under the name of Gradient Discretization Methods (see [12] for learning more) and many other extensions are underdevelopment (see [11] for instance). Let us state the following well-known Discrete Maximum Principle followed by a proof based upon a Geometrical Technique that seems new in this context to the best of our knowledge.

Theorem 3.5 (Discrete Maximum Principle) Let us suppose that Ω is a bounded open subset of $\mathbb{R}^2$, connected by polygonal arcs. Let its boundary Γ be the union of polygonal lines $\Gamma_k]_{k\in\mathbf{K}}$, where $\mathbf{K}$ is a finite subset of $\mathbb{N}$ (see Figure 1 below). The linear system (3.19) gets a unique solution that satisfies the following positivity property:

- If $I_T(f) \geq 0$ for all $T \in \mathcal{P}$ then

$$U_T \geq 0 \qquad \forall T \in \mathcal{T}. \tag{3.20}$$

Moreover the following discrete maximum principle holds :

- If there exists a control volume $\overline{T}$ from $\mathcal{P}$ such that

$$U_{\overline{T}} = 0 \equiv \min\{U_B;\ B \in \partial\mathcal{P}\}$$

then

$$U_T = 0 \qquad \forall T \in \mathcal{P}. \qquad \square \tag{3.21}$$

The originality of this work relies up on the technique exposed hereafter to prove that the solution to (3.19) meets the discrete Maximum Principle. This technique has been successfully applied to a new finite volume method introduced recently by A. Njifenjou, A. Toudna and S. Moussa in [11]. To the best of our knowledge the technique widely exposed in the literature (for proving the discrete maximum principle) is based up on algebraic arguments (see for instance [6,10]). We are going to develop geometric arguments for proving the discrete Maximum Principle stated above in Theorem 3.5.

IV. GEOMETRICAL TECHNIQUE FOR PROVING (3.20) AND (3.21)

♢ We have to first prove (3.20), that is:

If

$$\sum_{L\in\overline{\mathcal{P}},L\neq T} \frac{D^T D^L mes(\Gamma_T \cap \Gamma_L)}{D^T dist(x_L,T) + D^L dist(x_T,L)}[U_T - U_L] +$$

$$+ \sum_{L\in\overline{\mathcal{P}},L\neq T} [U_T \max\{\psi_{\sigma,T},0\} - U_L \max\{\psi_{\sigma,L},0\}] + U_T\, I_T(\mu) \geq 0 \quad \forall T \in \mathcal{P} \tag{4.1}$$

with

$$U_T = 0 \qquad \forall T \in \partial\mathcal{P} \tag{4.2}$$

then

$$U_T \geq 0 \qquad \forall T \in \mathcal{P}. \tag{4.3}$$

Let us set for all $(T,L) \in \mathcal{P} \times \overline{\mathcal{P}}$:

$$\alpha_{TL} \overset{def}{=} \frac{D^T D^L mes(\Gamma_T \cap \Gamma_L)}{D^T dist(x_L,T) + D^L dist(x_T,L)} \tag{4.4}$$

. Then notice that if T and L are adjacent control volumes i.e. Γ_T and Γ_L get a common edge, we have

$$\alpha_{TL} \succ 0. \tag{4.5}$$

and otherwise we have

$$\alpha_{TL} = 0. \tag{4.6}$$

In the sequel $\mathcal{V}_E$ denotes the set of control volumes from $\overline{\mathcal{P}}$ adjacent to a given control volume E from $\mathcal{P}$.

Let us start the proof with assuming that we have (4.1) and (4.2). We should deduce that (4.3) holds. Now let us set:

$$\begin{cases} U_{min}^{\overline{\mathcal{P}}} \overset{def}{=} \min\{U_T;\ T \textit{ browsing the set } \overline{\mathcal{P}}\} \\ \textit{and} \\ \overline{\mathcal{P}}^{min} \overset{def}{=} \{T \in \overline{\mathcal{P}} \ / \ U_T = U_{min}^{\overline{\mathcal{P}}}\}. \end{cases} \tag{4.7}$$

First of all we should notice that $U_{min}^{\overline{\mathcal{P}}}$ exists as $\{U_T;\ T \textit{ browsing the set } \overline{\mathcal{P}}\}$ is a finite subset of $\mathbb{R}$. Therefore $\overline{\mathcal{P}}^{min}$ is not an emptyset.

- If $\overline{\mathcal{P}}^{min} \cap \partial\mathcal{P} \neq \emptyset$, it is clear that the discrete Maximum Principle is satisfied. Indeed, denote by L a (degenerate) control-volume belonging to $\overline{\mathcal{P}}^{min} \cap \partial\mathcal{P}$. So we have

$$U_L = 0 \quad (\text{since } L \in \partial\mathcal{P}) \qquad \textit{and} \qquad U_L = U_{min}^{\overline{\mathcal{P}}} \quad (\text{since } L \in \overline{\mathcal{P}}^{min}). \tag{4.8}$$

Hence

$$U_T \geq 0 \qquad \forall\, T \in \mathcal{P}. \tag{4.9}$$

- We are going to geometrically prove that $\overline{\mathcal{P}}^{min} \cap \partial\mathcal{P} = \emptyset$ is *impossible*. Reasoning by the absurd let us suppose that:

$$\overline{\mathcal{P}}^{min} \cap \partial\mathcal{P} = \emptyset. \tag{4.10}$$

This assumption necessarily ensures that: $\overline{\mathcal{P}}^{min} \subset \mathcal{P}$ and $\overline{\mathcal{P}}^{min}$ is not empty. Let us *arbitrarily* consider a control volume $\overline{T}$ from $\overline{\mathcal{P}}^{min}$ (notice that $\overline{T}$ is not the closure of T). Since $\overline{T}$ necessarily belongs to $\mathcal{P}$, the assumption (4.1) applies for $T = \overline{T}$ and, thanks to definition (4.4) and relation (4.5), we get (with $\sigma \in \mathcal{E}_{\overline{T}} \cap \mathcal{E}_L$, if $\overline{T}$ and L adjacent):

$$0 \quad \leq \quad \sum_{L \in \mathcal{V}_{\overline{T}}} \underbrace{\alpha_{\overline{T}L}}_{\succ 0} \overbrace{[U_{\overline{T}} - U_L]}^{\leq 0} \quad + \quad \underbrace{I_{\overline{T}}(\mu)}_{\geq 0} \overbrace{U_{\overline{T}}}^{\leq 0} \ +$$

$$+ \sum_{L\in\overline{\mathcal{P}},L\neq\overline{T}} [U_{\overline{T}} \max\{\psi_{\sigma,\overline{T}},0\} - U_L \max\{\psi_{\sigma,L},0\}] \tag{4.11}$$

Let us prove the following lemma stating that the last summation in the right-hand side of the preceding inequality is in fact less than or equal to zero.

Lemma 4.1

$$\sum_{L\in\overline{\mathcal{P}},L\neq\overline{T}} [U_{\overline{T}} \max\{\psi_{\sigma,\overline{T}},0\} - U_L \max\{\psi_{\sigma,L},0\}] \leq 0 \tag{4.12}$$

where $\sigma = \Gamma_{\overline{T}} \cap \Gamma_L$.

Notice that if $\Gamma_{\overline{T}} \cap \Gamma_L = \emptyset$ the expression $[U_{\overline{T}} \max\{\psi_{\sigma,\overline{T}},0\} - U_L \max\{\psi_{\sigma,L},0\}]$ is zero.

Proof. The following equality is obvious :

$$\sum_{L\in\overline{\mathcal{P}},L\neq\overline{T}} [U_{\overline{T}} \max\{\psi_{\sigma,\overline{T}},0\} - U_L \max\{\psi_{\sigma,L},0\}] = \sum_{\sigma\in\mathcal{E}_{\overline{T}}} \overbrace{[U_{\overline{T}} - U_L]}^{\leq 0} \underbrace{\max\{\ _{\sigma,L},0\}}_{\geq 0} +$$

$$+ \sum_{\sigma\in\mathcal{E}_{\overline{T}}} U_{\overline{T}} [\max\{\psi_{\sigma,\overline{T}},0\} - \max\{\psi_{\sigma,L},0\}] . \tag{4.13}$$

The proof is ended if we show that the second summation in the right-hand side of the preceding equality is less than or equal to zero. That is

$$\sum_{\sigma\in\mathcal{E}_{\overline{T}}} U_{\overline{T}} [\max\{\psi_{\sigma,\overline{T}},0\} - \max\{\psi_{\sigma,L},0\}] \leq 0 .$$

This assertion is true. Indeed we have (since for all $\sigma = \Gamma_{\overline{T}} \cap \Gamma_L, \psi_{\sigma,\overline{T}} + \psi_{\sigma,L} = 0$ holds in virtue of the convection flux continuity):

$$\sum_{\sigma\in\mathcal{E}_{\overline{T}}} U_{\overline{T}} [\max\{\psi_{\sigma,\overline{T}},0\} - \max\{\psi_{\sigma,L},0\}] =$$

$$= \sum_{\sigma\in\mathcal{E}_{\overline{T}}} U_{\overline{T}} [\max\{\psi_{\sigma,\overline{T}},0\} - \max\{-\psi_{\sigma,\overline{T}},0\}] =$$

$$= \sum_{\sigma\in\mathcal{E}_{\overline{T}}} U_{\overline{T}} [\max\{\psi_{\sigma,\overline{T}},0\} + \min\{\psi_{\sigma,\overline{T}},0\}]$$

Therefore we get

$$\sum_{\sigma\in\mathcal{E}_{\overline{T}}} U_{\overline{T}} [\max\{\psi_{\sigma,\overline{T}},0\} - \max\{\psi_{\sigma,L},0\}] = \sum_{\sigma\in\mathcal{E}_{\overline{T}}} U_{\overline{T}}\, \psi_{\sigma,\overline{T}}$$

i.e.

$$\sum_{\sigma\in\mathcal{E}_{\overline{T}}} U_{\overline{T}}\,[\max\{\psi_{\sigma,\overline{T}},0\}\ -\ \max\{\psi_{\sigma,L},0\}]\ =\ U_{\overline{T}}\sum_{\sigma\in\mathcal{E}_{\overline{T}}}\psi_{\sigma,\overline{T}}$$

In virtue of definition (3.5) it is clear that

$$\sum_{\sigma\in\mathcal{E}_{\overline{T}}} U_{\overline{T}}\,[\max\{\psi_{\sigma,\overline{T}},0\}\ -\ \max\{\psi_{\sigma,L},0\}]\ =\ U_{\overline{T}}\sum_{\sigma\in\mathcal{E}_{\overline{T}}}\int_{\sigma}\psi\cdot\nu_{\sigma,\overline{T}}\,ds$$

It follows from Ostrogradski's theorem (called some times Divergence theorem) that

$$\sum_{\sigma\in\mathcal{E}_{\overline{T}}} U_{\overline{T}}\,[\max\{\psi_{\sigma,\overline{T}},0\}\ -\ \max\{\psi_{\sigma,L},0\}]\ =\ U_{\overline{T}}\int_{\overline{T}}\mathbf{div}(\psi)\,dx$$

Thanks to the assumption (1.6) and since $U_{\overline{T}}\ \leq\ 0$, it becomes obvious that

$$\sum_{\sigma\in\mathcal{E}_{\overline{T}}} U_{\overline{T}}\,[\max\{\psi_{\sigma,\overline{T}},0\}\ -\ \max\{\psi_{\sigma,L},0\}]\ \leq\ 0\,.$$

This ends the proof of the Lemma. ■

It obviously follows from inequalities (4.11) and the preceding Lemma as well that :

$$U_L\ =\ U_{\overline{T}}\qquad\qquad\forall\,L\in\mathcal{V}_{\overline{T}}\,. \tag{4.14}$$

For any pair of points from $\mathbb{R}^2$, with Cartesian coordinates x and y, define the subset $[x,y]$ of $\mathbb{R}^2$ in the following way :

$$[x,y]\ =\ \Big\{z\in\mathbb{R}^2\ /\ \exists 0\leq\theta\leq 1\text{ such that }z=\theta x+(1-\theta)y\Big\}. \tag{4.15}$$

Let us set:

$$\begin{cases}\mathcal{F}_{\overline{T}}\ =\ \Big\{x_\Gamma\in\Gamma\ /\ \exists\,x_{\overline{T}}\in\overline{T}\ \text{ such that }\ [x_{\overline{T}},x_\Gamma]\subset\overline{\Omega}\Big\}\\ \text{and}\\ \mathcal{S}_{\overline{T}}\ =\ \Big\{[x_{\overline{T}},x_\Gamma]\ /\ x_{\overline{T}}\in\overline{T}\text{ and }x_\Gamma\in\mathcal{F}_{\overline{T}}\Big\}.\end{cases} \tag{4.16}$$

Remark that $\mathcal{F}_{\overline{T}}$ is an infinite set and there is an obvious bijective mapping from $\mathcal{S}_{\overline{T}}$ onto $\overline{T}\times\mathcal{F}_{\overline{T}}$. So $\mathcal{S}_{\overline{T}}$ is also an infinite set. The set $\mathcal{S}_{\overline{T}}$ contains a finite subset $\mathcal{A}_{\overline{T}}$ made up of segments that pass through a mesh vertex or a mesh edge. So its complement $\mathcal{A}_{\overline{T}}^{C}$ in $\mathcal{S}_{\overline{T}}$ is also infinite. Thus there exists (at least) a segment $\Delta(\widetilde{x}_{\overline{T}},\widetilde{x}_\Gamma)$ from $\mathcal{A}_{\overline{T}}^{C}$, with extremities $\widetilde{x}_{\overline{T}}\in\overline{T}$ and $\widetilde{x}_\Gamma\in\Gamma$. In the sequel $\Delta(x_{\overline{T}},\widetilde{x}_\Gamma)$ is simply denoted by Δ since there is no risk of confusion. Let us set:

$$\overline{\mathcal{P}}_\Delta\ =\ \Big\{T\in\overline{\mathcal{P}}\ /\ T\cap\Delta\ \neq\ \emptyset\Big\}. \tag{4.17}$$

◦ The first important remark is that $\overline{\mathcal{P}}_\Delta$ contains at least two control volumes namely the control volume $\overline{T}$ belonging to $\mathcal{P}$ and a degenerate control volume T_Γ (belonging to $\partial\mathcal{P}$ of course) such that $\widetilde{x}_\Gamma\in T_\Gamma$.

◦ The second important remark straightly coming from (4.14) is that :

$$U_L = U_{\overline{T}} \quad \forall\, L \in \overline{\mathcal{P}}_\Delta. \tag{4.18}$$

From these two remarks we see that

$$U_{T_\Gamma} = U_{\overline{T}}, \quad \text{with} \quad T_\Gamma \in \partial\mathcal{P}.$$

Therefore we have the following result:

$$T_\Gamma \in \overline{\mathcal{P}}^{min} \cap \partial\mathcal{P}$$

which is in contradiction with the assumption (4.10). The proof of the Positivity Property (3.20) ends here.

♢ We have now to prove (3.21). For this purpose let us assume that there exists a control volume $\overline{T}$ from $\mathcal{P}$ such that

$$U_{\overline{T}} = 0 \equiv \min\{U_B;\, B \in \partial\mathcal{P}\}.$$

We shall deduce that

$$U_T = 0 \qquad \forall\, T \in \mathcal{P}. \tag{4.19}$$

Let us recall that a subset A of $\mathbb{R}^2$ is connected by polygonal arcs if and only if for any pair of points from A there exists a polygonal line inside $\overline{\Omega}$ joining these two points.

Let T be an *arbitrarily* chosen non degenerate control volumes i.e. $T \in \mathcal{P}$ and let $\mathcal{C}(\overline{T}, T)$ be the set of polygonal lines inside $\overline{\Omega}$ joining $\overline{T}$ to T. It is clear that $\mathcal{C}(\overline{T}, T)$ is an infinite set. Likewise it is clear that the subset of $\mathcal{C}(\overline{T}, T)$ denoted by $\mathcal{D}(\overline{T}, T)$ and made up of polygonal lines passing through a mesh vertex or involving a mesh edge is a finite set. So the complement $\mathcal{D}^C(\overline{T}, T)$ of $\mathcal{D}(\overline{T}, T)$ in $\mathcal{C}(\overline{T}, T)$ is an infinite set. Notice that any polygonal line from $\mathcal{D}^C(\overline{T}, T)$ is associated with a finite family of nondegenerate control volumes. Let us denote by $\Pi(\overline{T}, T)$ a polygonal line from $\mathcal{D}^C(\overline{T}, T)$. So there exists a finite sequence of nondegenerate control volumes $\{T_n\}_{n=1}^N$ associated with $\Pi(\overline{T}, T)$, where the numbering is such that for all $T \in \mathcal{P}$:

$$\begin{cases} T_1 = \overline{T}, \quad T_N = T \\ \text{and} \\ \forall\, 2 \le n \le N-1, \quad T_n \text{ is adjacent to } T_{n-1} \text{ and } T_{n+1}. \end{cases} \tag{4.20}$$

We know from the previous development of this proof that (see (4.14) above):

$$U_{T_n} = U_{T_{n+1}} \qquad \forall\, 1 \le n \le N-1$$

Thus, by transitivity of the equality relation we get what follows:

$$U_{\overline{T}} = U_T \qquad \forall\, T \in \mathcal{P}.$$

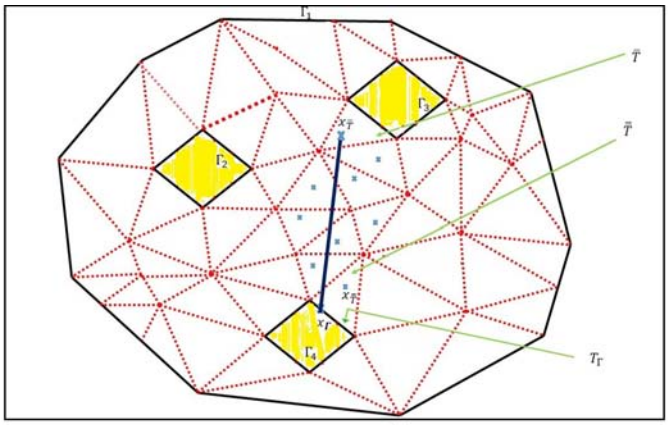

Figure: 1 Illustration of gridding defined over an open bounded subset Ω of $\mathbb{R}^2$, connected by polygonal arcs, with borders $\Gamma_k]_{k\in K}$ surrounding hollows represented by yellow quadrilaterals.

Declaration: We have no con ict of interests to declare.

REFERENCES:

1. H. Brezis, Functional Analysis, Sobolev Spaces and Partial Dierential Equations, Springer (2011).
2. F. Boyer, Analyse Numrique des Equations aux Drives Partielles, 2016-math, univ-toulouse.fr
3. C.M. Marle, Multiphase Flow in Porous Media, Editor: Technip, 2000.
4. A. Houpeurt, Mecanique desuides dans les milieux poreux: critiques etrecherches, Editor: Technip, 1974.
5. A. Njifenjou, Overview on conventional nite volumes for elliptic problems involving discontinuous di
   fusion coecients. Part I : Focus on the one dimension space models. Preprint ResearchGate, September 2022, DOI: 10.13140/RG.2.2.27472.17925
6. R. Eymard, Th. Gallouet and R. Herbin, Finite Volume Methods, HandBook of Numerical Analysis, Editors: P.G. Ciarlet and J. L. Lions, 2000.
7. A.H. Le and P. Omnes, An a Posteriori Error Estimation for the Discrete Duality Finite Volume Discretization of the Stokes Equations. Math. Model. Numer. Anal., 49, pp. 663693, 2015.
8. F. Hermeline, A nite volume method for approximating 3D diusion operators on general meshes, Journal of Computational Physics, Vol. 228, Issue 16, 2009.
9. I. Aavatsmark, Multi-point ux approximation methods for quadrilateralgrids. In: 9th International Forum on Reservoir Simulation, Abu Dhabi (2007).
10. A. Njifenjou, H. Donfack, I. Moukouop-Nguena, Analysis on general meshes of a discrete duality nite volume method for subsurface low problems, Computational Geosciences, 17, 391-415, 2013.
11. A. Njifenjou, A. Toudna Mansou and Moussa Sali, A New Second-order Maximum-principle-preserving Finite-volume Method for Flow Problems Involving Discontinuous Coecients, American Journal of Applied Mathematics; 12(4): 91 110, 2024.
12. J. Droniou, R. Eymard, Th. Gallout, C. Guichard and R. Herbin, The Gradient Discretization Methods, 2018, hal-01382358v7.
13. X. Blanc, F. Hermeline, E. Labourasse and J. Patela, High-order monotonenite-volume schemes for 1D elliptic problems, HAL Id: cea-03421015, March 2022.

14. J. Hyman, J. Morel, M. Shashkov, and S. Steinberg, Mimetic nite dierence methods for diusion equations, Computational Geosciences, 6(2002), 333 - 352.
15. C. Zhangxi, H. Guanren and M. Yuanle, Computational Methods for Multiphase Flows in Porous Media, SIAM book (2006).